

The non-Abelian geometry, topology, and dynamics of a nonreciprocal Su-Schrieffer-Heeger ladder

Ziyu Zhou,^{1,2,*} Zhi-Cong Xu,^{1,*} and Li-Jun Lang^{1,3,4,†}

¹*School of Physics, South China Normal University, Guangzhou 510006, China*

²*Guangzhou No.5 Middle School, Guangzhou 510000, China*

³*Guangdong Provincial Key Laboratory of Quantum Engineering and Quantum Materials, School of Physics, South China Normal University, Guangzhou 510006, China*

⁴*Key Laboratory of Atomic and Subatomic Structure and Quantum Control (Ministry of Education), School of Physics, South China Normal University, Guangzhou 510006, China*

(Dated: February 10, 2025)

Non-Hermiticity breaks down the adiabaticity and naturally leads to the non-Abelian behaviors in multi-band systems. Here we consider a multi-band, non-Hermitian ladder model with the two legs being the nonreciprocal Su-Schrieffer-Heeger chains. We thoroughly study how the non-Abelian geometry, topology, and dynamics emerge in this model at the onset of inter-leg coupling. Under periodic boundary conditions, by defining a gauge-invariant winding number for chiral symmetric systems, we analytically give the exact topological phase diagram. With the aid of underlying symmetries generalized for non-Hermitian systems, we further refine the phase diagram by the geometry of band structure. In the pseudo-Hermitian symmetric regime, we find that the stable non-Abelian dynamics of a Bloch state under an external constant force can be well described in some conditions of the force by the Wilson line constructed for non-Hermitian systems. Under open boundary conditions, we also find that the bulk-boundary correspondence survives in the thermodynamic limit but breaks down for finite-size systems with the leg-dependent non-Hermitian skin effect (NHSE), demonstrating the so-called critical NHSE, of which the decaying length of the bulk skin modes ξ varies with the system size L and is numerically verified to satisfy the scale-free power law $\xi \propto L$. Our work may stimulate more focuses on the non-Abelian properties of the non-Hermitian/open quantum systems.

In closed condensed matter systems, the geometry and topology of the band structure of a crystal is essential for understanding the electronic dynamics [1], where the key information comes from the Berry connection and the corresponding Berry phase of a Bloch state's adiabatic evolution in momentum space (i.e., k -space) of the crystal [2], especially in single bands. The geometry and topology of the subspace involving multiple bands (called the non-Abelian geometry and topology in the following) can be well described by the non-Abelian Berry connection (i.e., Wilczek-Zee connection) and the corresponding Wilson lines [3] if the gaps to the other bands are very large. In this case, the inter-band evolution (called non-Abelian dynamics in the following) in the subspace is no longer adiabatic, although the overall evolution in the subspace preserves the adiabaticity to the subspaces of other bands. Non-Abelian properties are common in condensed matter systems, such as in topological insulators [4, 5] and graphenes [6], which cannot be properly characterized by single-band quantities due to the existence of band degeneracy in k -space. The non-Abelian topology and dynamics have been traced by the Wilson lines or in cold-atom experiments [7, 8] and been studied with various theoretic methods [9–12].

On the other hand, in open quantum systems the short-time dynamics can be effectively described by

non-Hermitian Hamiltonians [13, 14]. The relaxation of the restriction of Hamiltonian's Hermiticity brings about many unique phenomena to non-Hermitian systems, such as parity-time (PT) symmetry breaking [15, 16], non-unitary evolution, exceptional points [17], etc., among which the emergence of non-Hermitian skin effects (NHSEs) [18] is the underlying reason to break down and reconstruct the bulk-boundary correspondence (BBC) [19–27], and thus deepens our understanding of topology and dynamics in non-Hermitian systems [13].

Since the intrinsic dissipation in non-Hermitian systems naturally breaks down the adiabaticity, leading to the mode switching between different bands, one may ask a question: what are the non-Abelian properties like in non-Hermitian systems? In Hermitian systems, one of the simplest theoretic models in one dimension with nontrivial non-Abelian properties is the two-leg Su-Schrieffer-Heeger (SSH) ladder [9] that couples two SSH chains as its two legs [28] and thus forms a four-band system. Different varieties of the two-leg SSH ladder are studied for broad theoretic interests [29–36]. Because of the nonsymmorphic symmetry, the band spectrum of a Hermitian model always has a band crossing point [37–41], which invalidates the single-band approximation and requires the non-Abelian quantities to describe the topology and dynamics. Here, we generalize this two-leg SSH ladder to the non-Hermitian regime that instead couples two nonreciprocal SSH chains with opposite NHSEs. Apparently, this non-Hermitian model is a four-band system like the Hermitian counterpart but with a complex spec-

* They contribute equally to this work.

† ljlang@sncu.edu.cn

trum, and the nonreciprocal legs offer the nontrivial non-Hermitian topology as well as the NHSEs. Therefore, the non-Hermitian two-leg SSH ladder offers a simple non-Hermitian platform to investigate the non-Abelian properties of non-Hermitian systems. In addition, the coupling of two nonreciprocal SSH chains with different skin depths will lead to the so-called critical NHSE [42–45]. In this non-Hermitian two-leg SSH ladder, one may also observe how the non-Abelian properties emerge from the inter-leg coupling.

Although there have been several works on different aspects on non-Abelian properties of non-Hermitian systems, such as the quantum metric in pseudo-Hermitian symmetric phases [46], knots and Wilson lines of non-Hermitian bands [47], the PT symmetry breaking [48], non-Abelian Bloch dynamics [49], the gain/loss effect in spin-orbit coupled systems [50], and also some works related to other non-Hermitian two-leg ladders [51–57], no detailed analysis is found for the non-Abelian geometry, topology, and dynamics of the non-Hermitian two-leg SSH ladder with opposite NHSEs. Therefore, in this paper after introducing the effective non-Hermitian Hamiltonian from the Lindblad master equation in Sec. I, based on the symmetry analysis of the Hamiltonian in Sec. II, we analytically give the exact non-Abelian topological phase diagram with various geometries of band structure via a newly defined gauge-invariant winding number under periodic boundary conditions (PBCs) in Sec. III, numerically demonstrate and understand the non-Abelian dynamics in the pseudo-Hermitian symmetric regime under different strengths of the external constant force with the aid of non-Hermitian Wilson lines in Sec. IV, and verify the BBC under open boundary conditions (OBCs) in the thermodynamic limit and the critical NHSE for the finite-size systems with the scale-free power law after the onset of inter-leg coupling in Sec. V. Finally, Sec. VI summarizes the results.

I. EFFECTIVE HAMILTONIAN OF THE DISSIPATIVE TWO-LEG SSH LADDER

Here we couple the system, a two-leg SSH ladder [9] that is formed by two SSH chains relatively shifted by half unit cell, to the environment, as shown in the upper panel of Fig. 1(a). Under the Markov approximation, the dynamics can be well described by the Lindblad master equation [14] as follows:

$$\frac{d\hat{\rho}}{dt} = -i[\hat{H}, \hat{\rho}] - \sum_{j\sigma} (\hat{L}_{j\sigma}^\dagger \hat{L}_{j\sigma} \hat{\rho} + \hat{\rho} \hat{L}_{j\sigma}^\dagger \hat{L}_{j\sigma} - 2\hat{L}_{j\sigma} \hat{\rho} \hat{L}_{j\sigma}^\dagger), \quad (1)$$

where $\hat{\rho} = |\psi(t)\rangle\langle\psi(t)|$ is the density matrix operator of the state $|\psi(t)\rangle$. The system Hamiltonian,

$$\hat{H} = \sum_j [\kappa(\hat{a}_{j\uparrow}^\dagger \hat{b}_{j\uparrow} + \hat{b}_{j\downarrow}^\dagger \hat{a}_{j+1,\downarrow}) + \nu(\hat{b}_{j\uparrow}^\dagger \hat{a}_{j+1,\uparrow} + \hat{a}_{j\downarrow}^\dagger \hat{b}_{j\downarrow}) + (\chi_+ \hat{a}_{j\uparrow}^\dagger \hat{a}_{j\downarrow} + \chi_- \hat{b}_{j\uparrow}^\dagger \hat{b}_{j\downarrow}) + \text{H.c.}], \quad (2)$$

represents a two-leg SSH ladder with $\hat{s}_{j\sigma}^{(\dagger)}$ ($s = a, b$ and $\sigma = \uparrow, \downarrow$) being the annihilation (creation) operator at the s -sublattice site of the j th unit cell in leg- σ of the ladder, and system parameters $\{\kappa, \nu, \chi_\pm\}$, which are set real for simplicity, being the hopping strengths shown in Fig. 1(a). The jump operators are set as [58]

$$\hat{L}_{j\uparrow} = \sqrt{\delta} (\hat{a}_{j\uparrow} + i\hat{b}_{j\uparrow}), \quad \hat{L}_{j\downarrow} = \sqrt{\delta} (\hat{b}_{j\downarrow} - i\hat{a}_{j+1,\downarrow}). \quad (3)$$

For convenience, the master equation (1) can be rewritten as

$$\frac{d\hat{\rho}}{dt} = -i(\hat{H}_{\text{NH}}\hat{\rho} - \hat{\rho}\hat{H}_{\text{NH}}^\dagger) + 2\sum_{j,\sigma} \hat{L}_{j\sigma} \hat{\rho} \hat{L}_{j\sigma}^\dagger, \quad (4)$$

where the summation term is called the quantum jump term. One can use the effective non-Hermitian Hamiltonian, $\hat{H}_{\text{eff}} \equiv \hat{H} - i\sum_{j\sigma} \hat{L}_{j\sigma}^\dagger \hat{L}_{j\sigma}$, to capture the short-time dynamics before a quantum jump occurs, or can directly neglect the quantum jump term by the schemes of post-selection in experiments. In the explicit form, one can easily find that the effective Hamiltonian,

$$\begin{aligned} \hat{H}_{\text{eff}} &= \sum_j \{ \kappa_+ (\hat{a}_{j\uparrow}^\dagger \hat{b}_{j\uparrow} + \hat{a}_{j+1,\downarrow}^\dagger \hat{b}_{j\downarrow}) + \kappa_- (\hat{b}_{j\uparrow}^\dagger \hat{a}_{j\uparrow} \\ &\quad + \hat{b}_{j\downarrow}^\dagger \hat{a}_{j+1,\downarrow}) + [\nu(\hat{b}_{j\uparrow}^\dagger \hat{a}_{j+1,\uparrow} + \hat{a}_{j\downarrow}^\dagger \hat{b}_{j\downarrow}) + \chi_+ \hat{a}_{j\uparrow}^\dagger \hat{a}_{j\downarrow} \\ &\quad + \chi_- \hat{b}_{j\uparrow}^\dagger \hat{b}_{j\downarrow} + \text{H.c.}] \} - i\delta \sum_{j\sigma} (\hat{a}_{j\sigma}^\dagger \hat{a}_{j\sigma} + \hat{b}_{j\sigma}^\dagger \hat{b}_{j\sigma}) \\ &\equiv \hat{H}_{\text{NH}} - i\delta \hat{N}, \end{aligned} \quad (5)$$

is just a non-Hermitian generalization of the two-leg SSH ladder by including a nonreciprocal hopping denoted by $\kappa_\pm = \kappa \pm \delta$ and an overall loss denoted by the total particle number operator \hat{N} . Note that in our case, the nonreciprocal hoppings in two legs are reversed such that opposite NHSEs occur for two legs in the limit of vanishing inter-leg coupling.

Since the loss term only contributes an overall decaying factor to the dynamics, without loss of generality, in the following we just focus on the Hamiltonian \hat{H}_{NH} instead, as shown in the lower panel of Fig. 1(a).

II. SYMMETRIES OF THE COMPLEX BAND STRUCTURE

To obtain the spectrum in k -space, we take the discrete Fourier transform,

$$\hat{s}_{j\sigma} = \frac{1}{\sqrt{L}} \sum_{k \in \text{BZ}} e^{ikjd} \hat{s}_{k\sigma}, \quad (6)$$

where L is the number of unit cells, d is the length of the unit cell, and the summation is done over one Brillouin zone (BZ) with $k = 2\pi n/L$ ($n \in \text{Integer}$). In the following, we set $d = \nu = 1$ as the units of length and energy, respectively. The non-Hermitian Hamiltonian in Eq. (5)

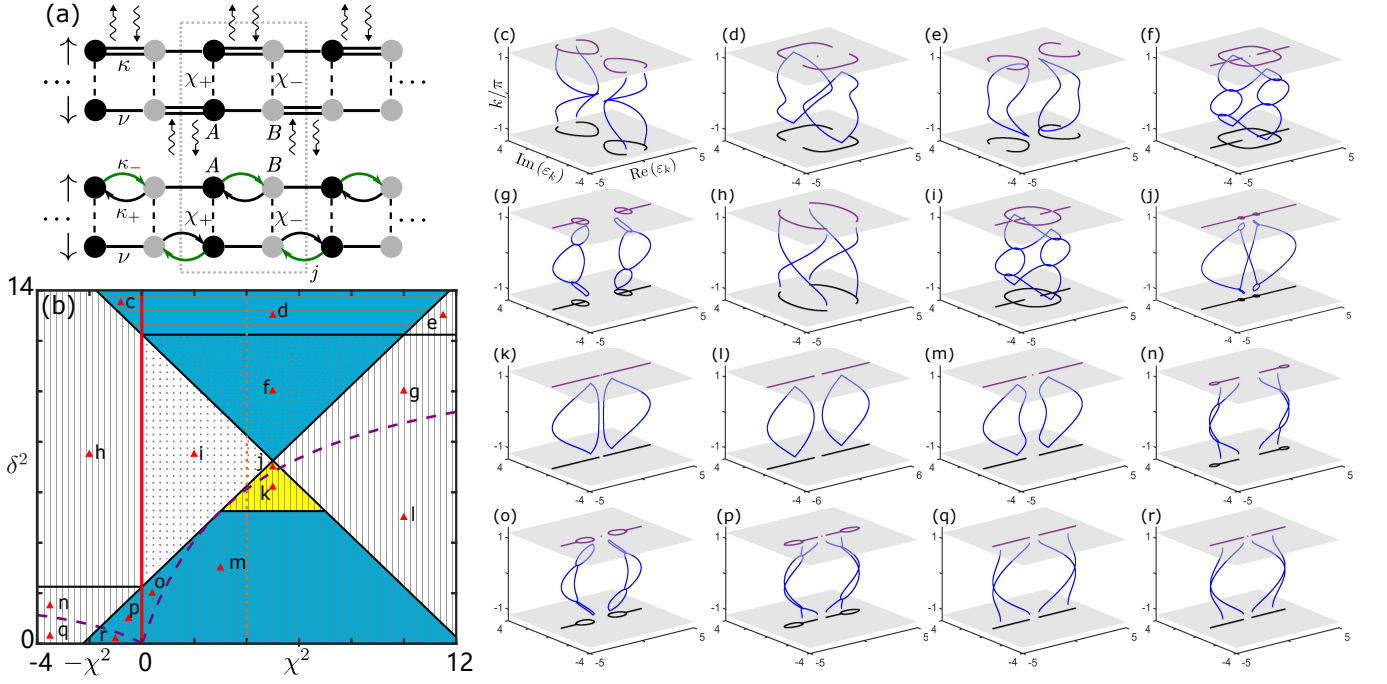


FIG. 1. (a) Upper panel: The sketch of a dissipative two-leg (denoted by \uparrow and \downarrow) SSH ladder coupled to the environment (denoted by the curly arrows), where κ, ν , and χ label the corresponding reciprocal hoppings. Lower panel: The sketch of the effective non-Hermitian Hamiltonian \hat{H}_{NH} formed by coupling two SSH chains with opposite nonreciprocal hoppings labeled by κ_{\pm} . The other parameters are the same as those in the upper panel. The gray dotted rectangle circles out the j th unit cell with A - and B -sublattice sites. (b) A typical topological phase diagram under PBCs characterized by the winding number $w = 1$ (blue), -1 (yellow), and 0 (white), with different geometries of band structures characterized by real line gaps (gray vertical lines), imaginary line gaps (gray horizontal lines), and point gaps (gray dots). The black solid lines indicate the gap closing/phase transition. The purple dashed line separates the purely real spectra from the others. The red vertical line at $\chi^2 = 0$ separates the negative ($-\chi^2$) and positive (χ^2) cases and also indicates the singularity caused by the critical NHSE under OBCs. The orange dotted line at $\chi^2 = 4$ is the parameter path for Fig.3(a). (c-r) Typical geometries of band structures for the points denoted by red triangles in (b) with parameters $(\chi^2, \delta^2) = (0.8, 13.5)$, $(5, 13)$, $(11.5, 13)$, $(5, 10)$, $(10, 10)$, $(2, 7.5)$, $(5, 7)$, $(5, 6.2)$, $(10, 5)$, $(3, 3)$, $(3.5, 1.5)$, $(0.4, 2)$, $(0.5, 1)$, $(3.5, 0.3)$, and $(1, 0.2)$, respectively. Bottom gray layers: the projection of the spectra under PBCs on the complex energy plane; Top gray layers: the corresponding spectra under OBCs for $L = 200$, where the isolated dots at zero energy in some gaps are the end states in the topological regimes.

can be transformed from the real space to k -space under PBCs:

$$\hat{H}_{\text{NH}} \equiv \hat{\psi}^\dagger H \hat{\psi} = \sum_{k \in \text{BZ}} \hat{\psi}_k^\dagger H_k \hat{\psi}_k, \quad (7)$$

where the bases in both spaces respectively read $\hat{\psi}^\dagger \equiv (\{\hat{a}_{j\uparrow}^\dagger, \hat{a}_{j\downarrow}^\dagger, \hat{b}_{j\uparrow}^\dagger, \hat{b}_{j\downarrow}^\dagger\})$ and $\hat{\psi}_k^\dagger = (\hat{a}_{k\uparrow}^\dagger, \hat{a}_{k\downarrow}^\dagger, \hat{b}_{k\uparrow}^\dagger, \hat{b}_{k\downarrow}^\dagger)$, and the Hamiltonian matrix in k -space is

$$H_k = \begin{pmatrix} \chi_+ & 0 \\ 0 & \chi_- \end{pmatrix} \otimes \sigma_x + \tau_+ \otimes \begin{pmatrix} \kappa_+ + e^{-ik} & 0 \\ 0 & 1 + \kappa_+ e^{-ik} \end{pmatrix} + \tau_- \otimes \begin{pmatrix} \kappa_- + e^{ik} & 0 \\ 0 & 1 + \kappa_- e^{ik} \end{pmatrix}. \quad (8)$$

Hereafter, $\tau_{x,y,z}$ and $\sigma_{x,y,z}$ are Pauli matrices acting on the sublattice (a, b) and the leg (\uparrow, \downarrow) spaces, respectively; τ_0 and σ_0 are corresponding identity matrices, and $\tau_{\pm} \equiv (\tau_x \pm i\tau_y)/2$.

When $\chi_+ = \chi_-$, due to the underlying symmetries of \hat{H}_{NH} in real space (the details can be referred to in Ap-

pendix B), the Hamiltonian matrix H_k in k -space satisfies the following relations inherited from the corresponding symmetries: (a) Time-reversal symmetry: $K H_k K = H_k^* = H_{-k}$ with K being the complex conjugation, due to the reality of all parameters of \hat{H}_{NH} ; (b) Sublattice symmetry: $C H_k C^\dagger = -H_k$ with $C \equiv \tau_z \otimes \sigma_z = C^\dagger = C^{-1}$, due to the bipartition of the ladder; (c) Pseudo-mirror symmetry: $M H_k M = H_{-k}^\dagger$ with $M \equiv \tau_x \otimes \sigma_0 = M^\dagger = M^{-1}$, which is a non-Hermitian generalization of the traditional mirror symmetry; (d) Inversion symmetry: $I_k H_k I_k^\dagger = H_{-k}$ with $I_k = \begin{pmatrix} 1 & 0 \\ 0 & e^{-ik} \end{pmatrix} \otimes \sigma_x$ satisfying $I_k^\dagger = I_k^{-1}$; (e) Pseudo-glide symmetry: $G_k H_k G_k^\dagger = H_k^\dagger$ with $G_k = \begin{pmatrix} 0 & e^{-ik} \\ 1 & 0 \end{pmatrix} \otimes \sigma_x$ satisfying $G_k^\dagger = G_k^{-1}$ and $G_k^2 = e^{-ik} I$ (I : identity matrix). These symmetries ensure that the eigenenergies of H_k belong to the D_{2h} point group in the composite 3D space spanned by the three 2-fold rotating axes of the k -axis, the real and the imag-

inary axes of the complex energy plane, which implies that the gap closing (indicating a phase transition) can only occur at the real or imaginary axes. The typical geometries of band structures are shown in Figs. 1(c)-1(r).

Additionally, besides the symmetries mentioned above, H_k also has an η_k -pseudo-Hermitian symmetry (the recap of pseudo-Hermiticity can be found in Appendix A) [13]:

$$\eta_k H_k \eta_k^{-1} = H_k^\dagger \quad (9)$$

with

$$\eta_k \equiv e^{ik/2} G_k = \begin{pmatrix} 0 & e^{-ik/2} \\ e^{ik/2} & 0 \end{pmatrix} \otimes \sigma_x = \eta_k^{-1} = \eta_k^\dagger. \quad (10)$$

This η_k -pseudo-Hermiticity of H_k guarantees that the eigenvalues are either purely real or appear in complex conjugate pairs, respectively defining the pseudo-Hermitian symmetric phase and the broken phase, according to whether or not the pair of the right and left column eigenvectors $u_k^{(r/l)}$ of H_k satisfies the relation $\eta_k u_k^{(r)} = \lambda_k u_k^{(l)}$ or equivalently $u_k^{(r)\dagger} \eta_k u_k^{(r)} = \lambda_k$ with λ_k being a nonzero real number. The corresponding pseudo-Hermiticity operation in real space is highly complex, unlike the previously mentioned symmetric operations, which can be referred to in Appendix B.

Compared with the Hamiltonian \hat{H} of the Hermitian two-leg SSH ladder, the dissipation-induced nonreciprocal hopping in \hat{H}_{HN} loosens some original symmetries, such as the mirror symmetry and the glide symmetry, to the corresponding pseudo ones, and also generalizes the time-reversal symmetry to the field of complex energies.

When $\chi_+ \neq \chi_-$, although the pseudo-mirror, the pseudo-glide, and the η_k -pseudo-Hermitian symmetries are broken, the time-reversal, the chiral, and the inversion symmetries are preserved. Therefore, the eigenenergies in the composite 3D space still belong to the D_{2h} point group and the gap closing can also occur only at the real or imaginary axes of the complex energy plane. The D_{2h} symmetry of the eigenenergies implies that the ladder possesses other hidden pseudo-Hermitian symmetry instead of the η_k -pseudo-Hermitian symmetries in Eq. (9) according to the statement in Appendix A, although we haven't found the explicit expression of the pseudo-Hermitian operation.

III. TOPOLOGICAL PHASE DIAGRAM WITH VARIOUS GEOMETRIES OF BAND STRUCTURE

To explore the non-Abelian topology (i.e., the topology involving a subspace or multiple bands) of this model, given that \hat{H}_{NH} respects the chiral symmetry, we define a gauge-invariant winding number under PBCs (which is essentially different from the commonly used gauge-dependent ones, see Appendix C):

$$w = \frac{1}{4\pi i} \int_{k \in \text{BZ}} \left[d \ln \det h_k^{(+)} - d \ln \det h_k^{(-)} \right], \quad (11)$$

where

$$h_k^{(\pm)} = \begin{pmatrix} \kappa_{\pm} + e^{\mp ik} & \chi_{\pm} \\ \chi_{\mp} & 1 + \kappa_{\mp} e^{\pm ik} \end{pmatrix} \quad (12)$$

are two 2×2 matrices of the following block off-diagonal Hamiltonian matrix

$$H_k^{(b)} = \begin{pmatrix} 0 & h_k^{(+)} \\ h_k^{(-)} & 0 \end{pmatrix}, \quad (13)$$

obtained from the Hamiltonian matrix (8) by changing the basis to $(\hat{a}_{k\uparrow}^\dagger \hat{b}_{k\downarrow}^\dagger \hat{b}_{k\uparrow}^\dagger \hat{a}_{k\downarrow}^\dagger)$. Define a function $d_k \equiv \det h_k^{(+)} = (2\kappa - \chi_+ \chi_-) + (\kappa^2 - \delta^2 + 1) \cos k + i(\kappa^2 - \delta^2 - 1) \sin k$, which generally forms an ellipse in the complex plane by scanning k , the polar angle with respect to the ellipse center, from 0 to 2π . Noting that $\det h_k^{(-)} = d_{-k}$, Eq. (11) becomes

$$w = \frac{1}{2\pi i} \int_{k \in \text{BZ}} d \ln d_k, \quad (14)$$

which depends on κ , δ^2 , and $\chi_+ \chi_-$. From the geometrical meaning of the winding number w , the topological phase with $w \neq 0$ must satisfy the following condition:

$$|2\kappa - \chi_+ \chi_-| < |\kappa^2 - \delta^2 + 1| \quad \text{and} \quad \kappa^2 - \delta^2 \neq 1, \quad (15)$$

and the topological phase boundaries are determined by the following formula:

$$\begin{aligned} \delta^2 &= (\kappa \pm 1)^2 \mp \chi_+ \chi_-, \\ \text{and } \delta^2 &= \kappa^2 - 1 \quad (\text{within } w \neq 0 \text{ regions}). \end{aligned} \quad (16)$$

Since w does not change if one simultaneously inverts the both signs of κ and $\chi_+ \chi_-$, one can only plot the topological phase diagram for $\kappa \geq 0$ with respect to $\chi_+ \chi_-$, as shown in Fig. 1(b).

Furthermore, one can analytically diagonalize H_k to get four energy bands:

$$\epsilon_k = \pm \sqrt{\alpha_k \pm \sqrt{\beta_k}}, \quad (17)$$

where the two ' \pm 's are uncorrelated, and the two quantities

$$\begin{aligned} \alpha_k &= \kappa^2 + 2\kappa \cos k + 1 + (\chi_+^2 + \chi_-^2)/2 - \delta^2, \\ \beta_k &= 4\delta^2(\cos^2 k - 1) + 2\cos k [\kappa(\chi_+^2 + \chi_-^2) \\ &\quad + (\kappa^2 - \delta^2 + 1)\chi_+ \chi_-] + (\chi_+^2 - \chi_-^2)^2/4 \\ &\quad + (\kappa^2 - \delta^2 + 1)(\chi_+^2 + \chi_-^2) + 4\kappa \chi_+ \chi_- \end{aligned} \quad (18)$$

are both real. Given the nested form of double-square-root in Eq. (17) with real quantities α_k and β_k , the geometry of band structures can be classified according to the complexity of bands (i.e., purely real, purely imaginary, and complex) or gap types (i.e., real line, imaginary line, and point). The corresponding conditions are shown in Table I. For simplicity but without the loss

Band Types ($\forall k$)	
Purely real	$\beta_k \geq 0$ & $\alpha_k \geq \sqrt{\beta_k}$
Purely imaginary	$\beta_k \geq 0$ & $\alpha_k < -\sqrt{\beta_k}$
Complex	others
Gap Types ($\forall k$)	
Real line	$(\beta_k \geq 0$ & $\alpha_k > \sqrt{\beta_k})$ or $(\beta_k < 0$ & $\alpha_k \neq 0)$
Imaginary line	$(\beta_k \geq 0$ & $\alpha_k < -\sqrt{\beta_k})$ or $\beta_k < 0$
Point	others

TABLE I. Classification of the geometry of band structures.

of typical geometries of band structures, in the following we mainly focus on the more symmetric cases of $|\chi_+| = |\chi_-| \equiv \chi > 0$, where we call $\chi_+ \chi_- = \pm \chi^2$ the positive and the negative cases, respectively. Thus, the quantities in Eq. (18) are reduced to

$$\begin{aligned} \alpha_k &= \kappa^2 + 2\kappa \cos k + 1 + \chi^2 - \delta^2, \\ \beta_k^{(\pm)} &= 2(1 \pm \cos k) [\chi^2(\kappa \pm 1)^2 - \delta^2(\chi^2 \mp 2 \cos k + 2)], \end{aligned} \quad (19)$$

where the “ \pm ” in $\beta_k^{(\pm)}$ corresponds to the positive and the negative cases, respectively.

From Eq. (17), we also know that any two bands touch in k -space must satisfy one of the following two conditions: (I) $\exists k \in \text{BZ}$, $\beta_k = 0$, which indicates an always-existing gapless point $k = \pi$ (0) for the positive (negative) case, and an inequality

$$\frac{\chi^2(\kappa \pm 1)^2}{\chi^2 + 4} \leq \delta^2 \leq (\kappa \pm 1)^2, \quad (20)$$

where the ‘ \pm ’ corresponds to the positive and the negative cases, respectively; (II) $\exists k \in \text{BZ}$, $\beta_k = \alpha_k^2$, which leads to the gapless equations for the positive case (i.e., $\chi_+ \chi_- = \chi^2$):

$$\delta^2 = \begin{cases} (\kappa - 1)^2 + \chi^2 \\ (\kappa + 1)^2 - \chi^2, & \chi^2 \leq (\kappa + 1)^2 \\ \kappa^2 - 1, & \kappa \geq 1 \text{ \& } 2(\kappa - 1) \leq \chi^2 \leq 2(\kappa + 1), \end{cases} \quad (21)$$

and for the negative case (i.e., $\chi_+ \chi_- = -\chi^2$):

$$\delta^2 = \begin{cases} (\kappa + 1)^2 + \chi^2 \\ (\kappa - 1)^2 - \chi^2, & \chi^2 \leq (\kappa - 1)^2 \\ \kappa^2 - 1, & \kappa \leq -1 \text{ \& } 2(-\kappa - 1) \leq \chi^2 \leq 2(-\kappa + 1). \end{cases} \quad (22)$$

Clearly, the gapless equations (21) and (22) are just Eq. (16) for the topological phase boundaries. Moreover, along with the up/lower bounds in Eq. (20), the phase diagram can be divided into regions with different geometries of band structures, as shown in Figs. 1(c)-1(r), which can also be derived from the conditions in Table I;

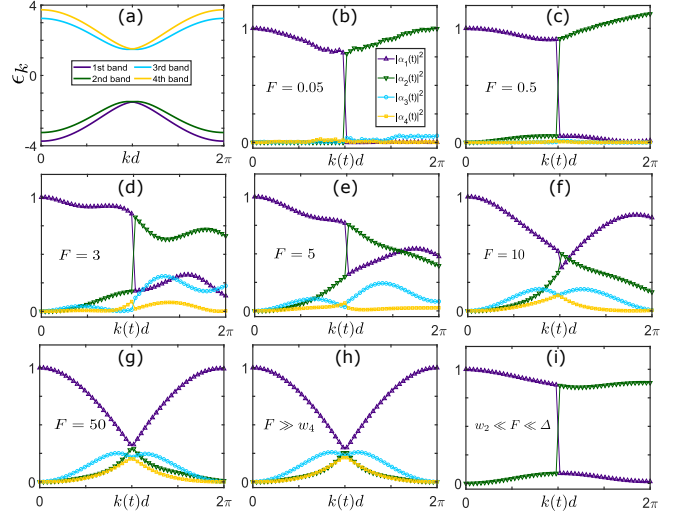


FIG. 2. (a) A typical purely real band structure with parameters $(\kappa, \chi^2, \delta^2) = (2.5, 0.06, 0.06)$ in the pseudo-Hermitian symmetric phase of the positive case. The characteristic quantities are $(w_2, \Delta, w_4) \approx (0.49, 2.97, 7.47)$. (b-g) The evolution of unnormalized populations $|\alpha_n(t)|^2$ in n th band given an initial state located at $k = 0$ of the lowest band in (a) for various strengths of the force $F = 0.05, 0.5, 3, 5, 10$, and 50 , respectively, which are all governed by Eq. (26). (h,i) The evolution of populations in each band given the same initial state as in (b-g) but using the four-band and two-band Wilson lines $W_{0 \rightarrow k}$ and $W_{0 \rightarrow k}^{(-)}$, governed by Eqs. (28) and (30), respectively. The numerical calculation is done by dividing the path $0 \rightarrow 2\pi$ into 49 equal pieces, and the details of method can be found in Appendix D.

in this model, there is no purely imaginary band structure for the positive and the negative cases. Notably, the lower bound of the inequality (20) is just the boundary of the purely real band structure, which only exists for

$$\delta^2 \leq \frac{\chi^2(\kappa \pm 1)^2}{\chi^2 + 4}, \quad (23)$$

where one can verify that $u_k^{(r)\dagger} \eta_k u_k^{(r)}$ is a nonzero real number for each k for the positive case, indicating the pseudo-Hermitian symmetric phases for all k 's. The symmetric phase in the negative case cannot be straightforwardly verified due to the lack of a simple expression of the pseudo-Hermitian operator, but one can also verify this using the more complex expression in Appendix A.

IV. NON-ABELIAN DYNAMICS UNDER AN EXTERNAL CONSTANT FORCE IN THE PSEUDO-HERMITIAN SYMMETRIC REGIME

Since there always exists a band touching point at $k = \pi$ (0) for the positive (negative) case, the adiabatic evolution for a single band cannot work any more in k -space. Here we focus on the non-Abelian dynamics (i.e.,

the dynamics involving multiple bands) in the pseudo-Hermitian symmetric phase where all bands are real and thus the dynamics is stable without amplitudes decaying or amplifying in the long-time limit, while in the cases with complex bands, the eigenstates with eigenenergies of the largest imaginary parts will dominate in the long-time limit.

To investigate the non-Abelian dynamics in k -space, we add an external constant force F along, say, the right direction of the ladder, and the evolution satisfies the time-independent Schrödinger equation ($\hbar = 1$) [7]:

$$i\partial_t|\psi(t)\rangle = (\hat{H}_{\text{HN}} - F\hat{X})|\psi(t)\rangle, \quad (24)$$

where $\partial_t \equiv \partial/\partial t$ and for simplicity the position operator \hat{X} is defined only with respect to the positions of unit cells:

$$\hat{X} : \hat{a}_{j\sigma}^{(\dagger)} \rightarrow j\hat{a}_{j\sigma}^{(\dagger)}, \quad \hat{b}_{j\sigma}^{(\dagger)} \rightarrow j\hat{b}_{j\sigma}^{(\dagger)}. \quad (25)$$

The initial state is set as the superposition of Bloch states at k_0 , i.e., $|\psi(0)\rangle = \sum_{n=1}^4 \alpha_n(0)|u_{k_0n}^{(r)}\rangle$, where $\alpha_n(t)$ is the amplitude of the Bloch right state $|u_{k_0n}^{(r)}\rangle$ of \hat{H}_{NH} in the n th band at time t , and we normalize the coefficients at $t = 0$ by $\sum_n |\alpha_n(0)|^2 = 1$. With the ansatz that the initial state uniformly evolves to another superposition state $|\psi(t)\rangle = \sum_{n=1}^4 \alpha_n(t)|u_{k(t),n}^{(r)}\rangle$ at $k(t) = k_0 + Ft$, the solution to Eq. (24) is as follows:

$$\alpha(t) = \mathcal{P} \exp \left\{ -i \int_{k_0}^k dk (\Lambda_k/F + A_k) \right\} \alpha(0), \quad (26)$$

where $\alpha(t) = (\alpha_1(t), \alpha_2(t), \alpha_3(t), \alpha_4(t))^T$, \mathcal{P} is the path-ordered operator, and

$$A_{k(t)} = -iU_k^{-1}\partial_k U_k|_{k=k(t)} \quad (27)$$

is the non-Hermitian non-Abelian Berry connection for the whole bands with the matrices U_k and Λ_k being defined in the eigenvalue decomposition $U_k^{-1}H_k U_k = \Lambda_k \equiv \text{diag}(\epsilon_{k1}, \epsilon_{k2}, \epsilon_{k3}, \epsilon_{k4})$. Note that the normalization of $\alpha(t)$ at $t \neq 0$ does not hold in general due to the non-Hermiticity of \hat{H}_{NH} and thus the non-unitary evolution of Eq. (26). The detailed derivation of Eq. (26) and the numerical method to solve it can be referred to in Appendix D.

Equation (26) shows that the dynamics is closely related to the Berry connection A_k . When $F \gg w_4$, where w_4 is the maximum energy difference between the highest and the lowest bands (i.e., the total band width), A_k dominates the evolution and all four bands can be regarded as being degenerate in the whole BZ. Thus, Eq. (26) reduces to

$$\begin{aligned} \alpha(t) &\approx \mathcal{P} \exp \left[-i \int_{k_0}^k dk A_k \right] \alpha(0) \\ &\equiv W_{k_0 \rightarrow k} \alpha(0) = U_k^{-1} U_{k_0}, \end{aligned} \quad (28)$$

where

$$W_{k_0 \rightarrow k} \equiv \mathcal{P} \exp \left[-i \int_{k_0}^k dk A_k \right] \quad (29)$$

is a four-band Wilson line for non-Hermitian systems along the path from k_0 to k in k -space [50]. Equation (28) means that the evolution only depends on the start and the final points, regardless of the path's selection, as shown in Fig. 2(h), which reproduces the evolution by Eq. (26) under a very strong force, as shown in Fig. 2(g).

When $w_2 \ll F \ll \Delta$, where w_2 is the maximum energy difference between the lowest/highest two bands and Δ is the minimum energy difference (i.e., the gap) between the middle two bands, the lowest/highest two bands can be approximated as being degenerate in the whole BZ and the excitation to the other two bands can be ignored, that is, the dynamics can be considered as an adiabatic evolution in the subspace of the lowest/highest two bands. Thus, Eq. (26) can be approximately decoupled into two independent evolutions in each subspace:

$$\begin{aligned} \alpha^{(\pm)}(t) &\approx \mathcal{P} \exp \left[-i \int_{k_0}^k dk A_k^{(\pm)} \right] \alpha^{(\pm)}(0) \\ &\equiv W_{k_0 \rightarrow k}^{(\pm)} \alpha^{(\pm)}(0), \end{aligned} \quad (30)$$

where (\pm) means the upper/lower 2×2 diagonal blocks in the labeled matrices and 2×1 blocks in labeled column vectors. In this case, the non-Abelian dynamics is well described by the two-band Wilson lines for non-Hermitian systems [50] in corresponding subspaces:

$$W_{k_0 \rightarrow k}^{(\pm)} \equiv \mathcal{P} \exp \left[-i \int_{k_0}^k dk A_k^{(\pm)} \right], \quad (31)$$

as shown in Fig. 2(i), which is similar to the evolution by Eq. (26) under a medium force, as shown in Fig. 2(c).

The non-Abelian dynamics for other strengths of the force cannot be well captured by Wilson lines, as shown in other cases of Fig. 2. The details of the numerical method for calculating the two Wilson lines can be found in Appendix D.

V. BULK-BOUNDARY CORRESPONDENCE AND THE CRITICAL NHSE

To investigate whether the ladder satisfies the BBC, we numerically calculate the spectra under OBCs with $L = 400$ unit cells, as shown in top layers of Figs. 1(c)-1(r), and find that except for the topological zero-mode end states, which are protected by the chiral symmetry, the bulk spectra are identical to those under PBCs (the bottom layers in Figs. 1(c)-1(r)), indicating the survival of the BBC in this ladder. In addition, we also numerically calculate the open-bulk winding number in real space under OBCs [50, 58]:

$$w_r = \frac{1}{8L'} \text{tr}' \hat{C} \hat{Q} [\hat{Q}, \hat{X}], \quad (32)$$

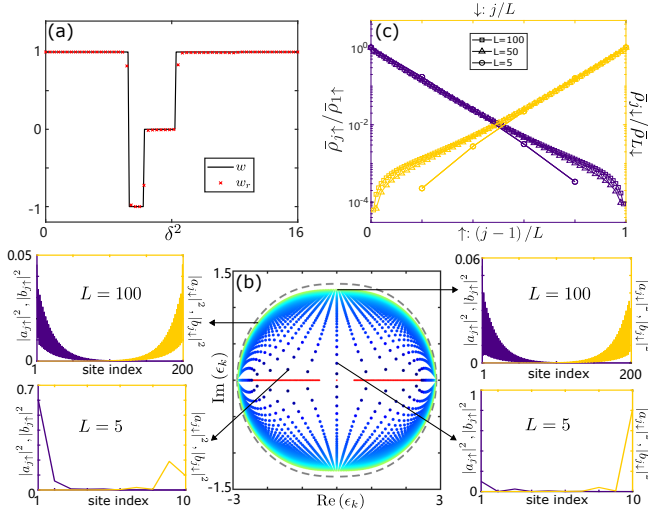


FIG. 3. (a) Comparison between the winding number w (black solid line) under PBCs and the open-bulk winding number w_r (red crosses) under OBCs along the orange dotted line at $\chi = 2$ in Fig. 1(b), where the parameters for calculating w_r are $(L, L', l) = (200, 160, 20)$. (b) The spectrum flow in complex energy plane under OBCs for various unit-cell numbers from $L = 5$ to 100 (from dark blue to light green dots) at weak inter-leg coupling $\chi = 0.01$ of the positive case. The spectrum (two red solid lines with dots in between) under OBCs without inter-leg coupling for $L = 100$ and the spectrum (gray dashed curve) under PBCs at $\chi = 0.01$ of the positive case are plotted for reference. Insets: Typical density distributions of bulk and end eigenstates in leg- \uparrow (purple) and leg- \downarrow (yellow) for several system sizes indicated by the arrows. The other parameters are $(\kappa, \delta) = (2.5, 2)$. (c) The averaged density distributions versus the scaled unit-cell index for $L = 5$ (circles), 50 (triangles), and 100 (squares) in leg- \uparrow (purple) and leg- \downarrow (yellow).

where \hat{C} is the chiral operator, $\hat{Q} \equiv \sum_n [|\phi_n^{(r)}\rangle\langle\phi_n^{(l)}| - \hat{C}|\phi_n^{(r)}\rangle\langle\phi_n^{(l)}|\hat{C}]$ is the “ Q -matrix” operator constructed by the n th chiral-operation paired right/left eigenstates $\{|\phi_n^{(r,l)}\rangle, \hat{C}|\phi_n^{(r,l)}\rangle\}$ of \hat{H}_{NH} under OBCs, and the primed trace means that the trace is done over a central $L' = L - 2l$ unit cells out of the whole L unit cells of the ladder with l unit cells being cut off from each end of the ladder when the numerical calculation is executed to avoid the boundary effects. The numerical results in Fig. 3(a) show that w_r is close to w for large systems, which hints that there is no BBC breaking and thus no skin effect in the thermodynamic limit $L \rightarrow \infty$. This can also be reflected by the winding number for energy under PBCs [22, 59]:

$$w_e = \frac{1}{2\pi i} \int_{k \in \text{BZ}} d \ln \det(H_k - \epsilon_r I), \quad (33)$$

where ϵ_r is an arbitrary reference point in the complex energy plane and I is the identity matrix. In our model, that $w_e = 0$ is always satisfied due to the inversion symmetry that enforces the energy spectrum to be symmetric with respect to $k = 0$ plane, leading to the relation

$$\det(H_{-k} - \epsilon_r I) = \det(H_k - \epsilon_r I).$$

However, when the inter-leg coupling vanishes (i.e., $\chi = 0$), the ladder is decoupled into two independent nonreciprocal SSH chains, which are well known for the breakdown of BBC and the emergence of NHSEs under OBCs. This indicates that in the thermodynamic limit, the BBC is abruptly restored with the introduction of an infinitesimal inter-leg coupling, which is called the critical NHSE [42]. The critical NHSE leads to a noticeable alteration of the energy spectra and eigenstates under OBCs in the weak inter-leg coupling limit as the system size increases, as shown in Fig. 3(b). When the size is small, the energy spectra and eigenstates are close to those of the decoupled nonreciprocal SSH chains under OBCs, i.e., the spectra are curve/line-like and the eigenstates demonstrate NHSEs, indicating that the coupling effects are negligible; when the size becomes larger, they converge to those under PBCs, i.e., the curve/line-like spectra expand to loops and the eigenstates tend to be delocalized without NHSEs as Bloch waves, indicating that the weak coupling becomes stronger in the thermodynamic limit. Quantitatively, for a finite-size weakly inter-leg coupled ladder under OBCs, the distribution of bulk eigenstates remain the exponential form $|\phi_j|^2 \propto e^{-|j-j_b|/\xi}$ of the skin bulk states of the nonreciprocal SSH chain, localized in the boundary unit cell j_b , but the decaying length ξ of the amplitude ϕ_j is size-dependent and satisfies the scale-free power law [42, 43]: $\xi(L) \propto L^c$, unlike the nonreciprocal SSH chain, where $\xi^{-1} = \frac{1}{2} \ln |\kappa_+/\kappa_-|$ is size-independent [18]. To show the power law, we define the averaged density distributions in leg- σ ($\sigma = \uparrow$ and \downarrow) for certain system size with unit-cell number L :

$$\bar{\rho}_{j\sigma} \equiv \frac{1}{L} \sum_{n=1}^L (|a_{j\sigma n}|^2 + |b_{j\sigma n}|^2), \quad (34)$$

where the amplitudes $a_{j\sigma n}$ and $b_{j\sigma n}$ are defined in the eigenvalue equation $H\phi_n^{(r)} = \epsilon_n \phi_n^{(r)}$ with the n th right column eigenvector $\phi_n^{(r)} = \{a_{j\uparrow n}, a_{j\downarrow n}, b_{j\uparrow n}, b_{j\downarrow n}\}^T$. Figure 3(c) shows the averaged density distributions $(\bar{\rho}_{j\uparrow}/\bar{\rho}_{1\uparrow}, \bar{\rho}_{j\downarrow}/\bar{\rho}_{L\downarrow})$ normalized by the corresponding localized boundary values versus the scaled unit cell index j/L for different system sizes. The collapse into the same lines for respectively upper and lower legs verify the scale-free power law with the power $c = 1$.

In addition, the critical NHSEs also have impact on the end states. Since the zero-mode end state protected by the chiral symmetry appears under OBCs when $\delta^2 < (>) \kappa^2 - 1$ for the nonreciprocal SSH chain with (non-)reciprocal unit cells being the boundary cells [18], in the decoupled case the two relatively shifted nonreciprocal SSH chains as a whole always have end states under OBCs with an arbitrary kind of boundary cells. This means that the topological end states in small-sized ladder with weak inter-leg couplings under OBCs may evolve into the bulk states of a topologically trivial phase in the thermodynamic limit, as shown in the insets of Fig. 3(b).

Now one may notice that the topological phase diagram in Fig. 1(b) is singular at $\chi^2 = 0$ (the gray vertical line) in the thermodynamic limit.

It is apparent that if we add a leg-dependent potential, the NHSE under OBCs along with the breakdown of BBC will return in the thermodynamic limit, with NHSEs depending on the eigenenergies, and thus the so-called bipolar NHSE will be naturally realized [58, 60].

VI. CONCLUSION

In conclusion, we thoroughly investigate the non-Abelian geometrical, topological and dynamical properties of an effective non-Hermitian description of a dissipative two-leg SSH ladder, i.e., a ladder of coupling two relatively shifted SSH chains with opposite nonreciprocal hoppings. We give the exact topological phase diagram characterized by defining a gauge-invariant winding number under PBCs for chiral symmetric multi-band systems, along with the various geometries of band struc-

ture based on the underlying symmetries of the ladder. The evolution of a Bloch state under an external constant force is also investigated in the pseudo-Hermitian symmetric regime to reveal the non-Abelian dynamics in the non-Hermitian multi-band subspace. Under OBCs, the BBC is found conserved for the non-Abelian topology in the thermodynamic limit of the ladder, but the critical NHSEs lead to the leg-dependent boundary localization of bulk states in finite-sized systems, obeying the scale-free law of the decaying length $\xi(L) \propto L$.

ACKNOWLEDGMENTS

This work was supported by the National Key Research and Development Program of China (Grant No. 2022YFA1405304), the Guangdong Basic and Applied Basic Research Foundation (Grant No. 2024A1515010188), the National Natural Science Foundation of China (Grant No. 11904109), and the Startup Fund of South China Normal University.

-
- [1] D. Xiao, M.-C. Chang, and Q. Niu, *Rev. Mod. Phys.* **82**, 1959 (2010).
 - [2] M. V. Berry, *Proceedings of the Royal Society of London* **392**, 45 (1984).
 - [3] F. Wilczek and A. Zee, *Phys. Rev. Lett.* **52**, 2111 (1984).
 - [4] X.-L. Qi and S.-C. Zhang, *Rev. Mod. Phys.* **83**, 1057 (2011).
 - [5] M. Z. Hasan and C. L. Kane, *Rev. Mod. Phys.* **82**, 3045 (2010).
 - [6] A. H. Castro Neto, F. Guinea, N. M. R. Peres, K. S. Novoselov, and A. K. Geim, *Rev. Mod. Phys.* **81**, 109 (2009).
 - [7] T. Li, L. Duca, M. Reitter, F. Grusdt, E. Demler, M. Endres, M. Schleier-Smith, I. Bloch, and U. Schneider, *Science* **352**, 1094 (2016).
 - [8] S. Sugawa, F. Salces-Carcoba, Y. Yue, A. Putra, and I. B. Spielman, *npj Quantum Information* **7**, 144 (2021).
 - [9] S.-L. Zhang, Q. Zhou, S.-L. Zhang, and Q. Zhou, *Phys. Rev. A* **95**, 061601 (2017).
 - [10] Q. Chen, J. Cai, and S. Zhang, *Phys. Rev. A* **101**, 043614 (2020).
 - [11] M. Di Liberto, N. Goldman, and G. Palumbo, *Nature communications* **11**, 5942 (2020).
 - [12] T. Jiang, R.-Y. Zhang, Q. Guo, B. Yang, and C. Chan, *Physical Review B* **106**, 235428 (2022).
 - [13] Y. Ashida, Z. Gong, and M. Ueda, *Advances in Physics* **69**, 249 (2020).
 - [14] H.-P. Breuer and F. Petruccione, *The Theory of Open Quantum Systems* (Oxford University Press, Oxford, 2002).
 - [15] C. M. Bender and S. Boettcher, *Physical Review Letters* **80**, 5243 (1998).
 - [16] C. M. Bender, *Reports on Progress in Physics* **70**, 947 (2007).
 - [17] E. J. Bergholtz, J. C. Budich, and F. K. Kunst, *Rev. Mod. Phys.* **93**, 015005 (2021).
 - [18] S. Yao and Z. Wang, *Physical Review Letters* **121**, 086803 (2018).
 - [19] T. E. Lee, *Phys. Rev. Lett.* **116**, 133903 (2016).
 - [20] D. Leykam, K. Y. Bliokh, C. Huang, Y. Chong, and F. Nori, *Phys. Rev. Lett.* **118**, 040401 (2017).
 - [21] H. Shen, B. Zhen, and L. Fu, *Phys. Rev. Lett.* **120**, 146402 (2018).
 - [22] Z. Gong, Y. Ashida, K. Kawabata, K. Takasan, S. Higashikawa, and M. Ueda, *Phys. Rev. X* **8**, 031079 (2018).
 - [23] Y. Xiong, *Journal of Physics Communications* **2**, 035043 (2018).
 - [24] F. K. Kunst, E. Edvardsson, J. C. Budich, and E. J. Bergholtz, *Phys. Rev. Lett.* **121**, 026808 (2018).
 - [25] K. Yokomizo and S. Murakami, *Physical Review Letters* **123**, 066404 (2019).
 - [26] L. Jin and Z. Song, *Phys. Rev. B* **99**, 081103 (2019).
 - [27] C. H. Lee and R. Thomale, *Phys. Rev. B* **99**, 201103(R) (2019).
 - [28] W. P. Su, J. R. Schrieffer, and A. J. Heeger, *Phys. Rev. Lett.* **42**, 1698 (1979).
 - [29] K. Padavić, S. S. Hegde, W. DeGottardi, and S. Vishveshwara, *Phys. Rev. B* **98**, 024205 (2018).
 - [30] T. Yoshida, I. Danshita, R. Peters, and N. Kawakami, *Phys. Rev. Lett.* **121**, 025301 (2018).
 - [31] M. Kurzyna and T. Kwapiński, *Phys. Rev. B* **102**, 195429 (2020).
 - [32] A. A. Nersesyan, *Phys. Rev. B* **102**, 045108 (2020).
 - [33] Z. Qin, D.-H. Xu, Z. Ning, and R. Wang, *Phys. Rev. B* **108**, 195103 (2023).
 - [34] A. Padhan, S. Mondal, S. Vishveshwara, and T. Mishra, *Phys. Rev. B* **109**, 085120 (2024).
 - [35] R. Parida, A. Padhan, and T. Mishra, *Phys. Rev. B* **110**, 165110 (2024).
 - [36] K. Sabour and Y. V. Kartashov, *Opt. Lett.* **49**, 3580 (2024).

- [37] S. M. Young and C. L. Kane, Phys. Rev. Lett. **115**, 126803 (2015).
- [38] C. Fang and L. Fu, Phys. Rev. B **91**, 161105 (2015).
- [39] K. Shiozaki, M. Sato, and K. Gomi, Phys. Rev. B **91**, 155120 (2015).
- [40] V. M. Martinez Alvarez, J. E. Barrios Vargas, and L. E. F. Foa Torres, Phys. Rev. B **97**, 121401 (2018).
- [41] C. Yin, H. Jiang, L. Li, R. Lü, and S. Chen, Phys. Rev. A **97**, 052115 (2018).
- [42] L. Li, C. H. Lee, S. Mu, and J. Gong, Nature communications **11**, 5491 (2020).
- [43] K. Yokomizo and S. Murakami, Phys. Rev. B **104**, 165117 (2021).
- [44] S. M. Rafi-Ul-Islam, Z. B. Siu, H. Sahin, C. H. Lee, and M. B. A. Jalil, Phys. Rev. Res. **4**, 013243 (2022).
- [45] G.-J. Liu, J.-M. Zhang, S.-Z. Li, and Z. Li, Phys. Rev. A **110**, 012222 (2024).
- [46] Y.-Q. Zhu, W. Zheng, S.-L. Zhu, and G. Palumbo, Phys. Rev. B **104**, 205103 (2021).
- [47] H. Hu and E. Zhao, Phys. Rev. Lett. **126**, 010401 (2021).
- [48] M. Ezawa, Phys. Rev. Res. **3**, 043006 (2021).
- [49] M. Parto, C. Leefmans, J. Williams, F. Nori, and A. Marandi, Nature Communications **14**, 1440 (2023).
- [50] Z.-C. Xu, Z. Zhou, E. Cheng, L.-J. Lang, and S.-L. Zhu, Science China Physics, Mechanics & Astronomy **65**, 283011 (2022).
- [51] X. M. Yang, X. Z. Zhang, C. Li, and Z. Song, Phys. Rev. B **98**, 085306 (2018).
- [52] J. S. Liu, Y. Z. Han, and C. S. Liu, Chinese Physics B **28**, 100304 (2019).
- [53] C. Wu, Z. Yang, J. Tang, N. Liu, and G. Chen, Phys. Rev. A **106**, 062206 (2022).
- [54] H. Tang, Z. Wang, L. Tang, D. Song, Z. Chen, and H. Buljan, APL Photonics **9**, 056102 (2024).
- [55] L. Qi, A.-L. He, H.-F. Wang, and Y. Liu, Phys. Rev. B **107**, 115107 (2023).
- [56] Z. Li, L.-W. Wang, X. Wang, Z.-K. Lin, G. Ma, and J.-H. Jiang, Nature Communications **15**, 10.1038/s41467-024-50776-1 (2024).
- [57] R.-J. Chen, G.-Q. Zhang, Z. Li, and D.-W. Zhang, Phys. Rev. A **110**, 043311 (2024).
- [58] F. Song, S. Yao, and Z. Wang, Physical Review Letters **123**, 170401 (2019).
- [59] H. Jiang, L.-J. Lang, C. Yang, S.-L. Zhu, and S. Chen, Phys. Rev. B **100**, 054301 (2019).
- [60] F. Qin, Y. Ma, R. Shen, and C. H. Lee, Phys. Rev. B **107**, 155430 (2023).
- [61] A. Mostafazadeh, Journal of Mathematical Physics **43**, 205 (2002).
- [62] A. Mostafazadeh, J. Math. Phys. **43**, 2814 (2002).
- [63] S. Ryu, A. P. Schnyder, A. Furusaki, and A. W. W. Ludwig, New Journal of Physics **12**, 065010 (2010).

Appendix A: Recap of the pseudo-Hermitian symmetry

To be self-consistent, we recap the concept of pseudo-Hermiticity symmetry in this section. Here, we assume that \hat{H} is a diagonalizable linear operator acting on the Hilbert space of dimension N , which has a set of complete biorthonormal right/left eigenvectors $\{|\phi_n^{(r/l)}\rangle\}$ and

a discrete spectrum $\{\epsilon_n\}$:

$$\langle\phi_n^{(l)}|\phi_m^{(r)}\rangle = \delta_{nm}, \quad \sum_{n=1}^N |\phi_n^{(r)}\rangle\langle\phi_n^{(l)}| = \hat{I},$$

$$\hat{H} = \sum_{n=1}^N \epsilon_n |\phi_n^{(r)}\rangle\langle\phi_n^{(l)}|. \quad (\text{A1})$$

\hat{H} is said to be η -pseudo-Hermitian [13] if it satisfies the relation:

$$\hat{H}^\dagger = \hat{\eta}\hat{H}\hat{\eta}^{-1}, \quad (\text{A2})$$

where $\hat{\eta}$ is a Hermitian invertible operator. If there exists one $\hat{\eta}$ such that \hat{H} is η -pseudo-Hermitian, \hat{H} is said to be pseudo-Hermitian [13].

This relation implies that the eigenvalues of \hat{H} are either real or appear in complex conjugate pairs. It can be proved as follows:

$$\hat{H}^\dagger \hat{\eta} |\phi_n^{(r)}\rangle = \hat{\eta} \hat{H} |\phi_n^{(r)}\rangle = \epsilon_n \hat{\eta} |\phi_n^{(r)}\rangle, \quad (\text{A3})$$

which implies that $\hat{\eta} |\phi_n^{(r)}\rangle$ is also a left eigenvector of \hat{H} with the eigenvalue ϵ_n^* . Furthermore, the identity

$$0 = \langle\phi_n^{(r)}|\hat{H}^\dagger \hat{\eta}|\phi_n^{(r)}\rangle - \langle\phi_n^{(r)}|\hat{H}\hat{\eta}|\phi_n^{(r)}\rangle$$

$$= \langle\phi_n^{(r)}|\hat{\eta}|\phi_n^{(r)}\rangle(\epsilon_n - \epsilon_n^*), \quad (\text{A4})$$

shows that the eigenvalues are either real ($\epsilon_n^* = \epsilon_n$) or appear in complex conjugate pairs ($\epsilon_n \neq \epsilon_n^*$) with $\langle\phi_n^{(r)}|\hat{\eta}|\phi_n^{(r)}\rangle = 0$. For eigenvectors $|\phi_n^{(r)}\rangle$ with real eigenvalues, if there is no degeneracy, it implies that $\langle\phi_n^{(r)}|\hat{\eta}|\phi_n^{(r)}\rangle \neq 0$, in which case the eigenvectors are called η -pseudo-Hermitian symmetric states; while for eigenvectors $|\phi_n^{(r)}\rangle$ with non-real eigenvalues, it implies that $\langle\phi_n^{(r)}|\hat{\eta}|\phi_n^{(r)}\rangle = 0$, in which case the eigenvectors are called η -pseudo-Hermitian broken states. For the degenerate eigenvectors with real eigenvalues, we can choose any superposition $|\phi\rangle$ to get any value of $\langle\phi|\hat{\eta}|\phi\rangle$. That the spectrum becomes non-real from real accompanied by the change of $\langle\phi_n^{(r)}|\hat{\eta}|\phi_n^{(r)}\rangle$ from nonzero to zero is called the pseudo-Hermitian symmetry breaking.

Inversely, any Hamiltonian with either real or complex conjugate paired eigenvalues are pseudo-Hermitian. According to this, Eq. (A1) can be generally divided into two parts:

$$\hat{H} = \sum_{\text{Im } \epsilon_n = 0} \epsilon_n |\phi_n^{(r)}\rangle\langle\phi_n^{(l)}|$$

$$+ \sum_{\text{Im } \epsilon_n > 0} (\epsilon_n |\phi_n^{(r)}\rangle\langle\phi_n^{(l)}| + \epsilon_n^* |\tilde{\phi}_n^{(r)}\rangle\langle\tilde{\phi}_n^{(l)}|), \quad (\text{A5})$$

where $|\tilde{\phi}_n^{(r/l)}\rangle$ is the counterpart eigenvectors to $|\phi_n^{(r/l)}\rangle$. A set of $\tilde{\eta}$'s can be easily expressed using the eigenstates

[61]:

$$\begin{aligned}\hat{\eta} &\equiv \sum_{\text{Im } \epsilon_n=0} \sigma_n |\phi_n^{(l)}\rangle \langle \phi_n^{(l)}| \\ &+ \sum_{\text{Im } \epsilon_n>0} (|\tilde{\phi}_n^{(l)}\rangle \langle \phi_n^{(l)}| + |\phi_n^{(l)}\rangle \langle \tilde{\phi}_n^{(l)}|), \\ \hat{\eta}^{-1} &\equiv \sum_{\text{Im } \epsilon_n=0} \sigma_n |\phi_n^{(r)}\rangle \langle \phi_n^{(r)}| \\ &+ \sum_{\text{Im } \epsilon_n>0} (|\phi_n^{(r)}\rangle \langle \tilde{\phi}_n^{(r)}| + |\tilde{\phi}_n^{(r)}\rangle \langle \phi_n^{(r)}|),\end{aligned}\quad (\text{A6})$$

where $\sigma_n = \pm 1$ can be arbitrarily assigned for different n . It can be easily verified that the pseudo-Hermiticity holds with the \hat{H} and $\hat{\eta}$ in Eqs. (A5) and (A6). Apparently, there may be many $\hat{\eta}$'s satisfying Eq. (A2).

The pseudo-Hermiticity does not ensure the reality of the spectrum. Actually, it is neither the sufficient nor the necessary condition for the reality of the spectrum. It is well known that any Hermitian operator has a real spectrum. Thus, the non-Hermitian operator \hat{H} with the real spectrum must be related to a Hermitian operator \hat{H}_h with the same spectrum by a similarity transformation \hat{O} :

$$\hat{H}_h = \hat{O}\hat{H}\hat{O}^{-1}.\quad (\text{A7})$$

The \hat{O} can be easily constructed using the eigenvectors $|\phi_n\rangle$ and $|\phi_n^{(r/l)}\rangle$ of \hat{H}_h and \hat{H} , respectively, yielding [62]

$$\hat{O} = \sum_n |\phi_n\rangle \langle \phi_n^{(l)}|, \quad \hat{O}^{-1} = \sum_n |\phi_n^{(r)}\rangle \langle \phi_n|.\quad (\text{A8})$$

From Eq. (A7), the Hermiticity $\hat{H}_h^\dagger = \hat{H}_h$ requires that

$$(\hat{O}^\dagger)^{-1} \hat{H}^\dagger \hat{O}^\dagger = \hat{O} \hat{H} \hat{O}^{-1},\quad (\text{A9})$$

and then we have

$$\hat{H}^\dagger = (\hat{O}^\dagger \hat{O}) \hat{H} (\hat{O}^\dagger \hat{O})^{-1},\quad (\text{A10})$$

which is just the $O^\dagger O$ -pseudo-Hermiticity of \hat{H} . This means that the operator with real spectrum must be $O^\dagger O$ -pseudo-Hermitian. The inverse statement can also be easily proved. Thus, the necessary and sufficient condition for an operator with real spectrum is the $O^\dagger O$ -pseudo-Hermiticity with \hat{O} being an invertible linear operator, that is, there must be a special η -pseudo-Hermiticity of \hat{H} with $\hat{\eta} = \hat{O}^\dagger \hat{O}$ [13].

As a comparison, \hat{H} is said to be *quasi-Hermitian* [13] if there exists one positive-definite Hermitian (not necessarily invertible) operator $\hat{\xi}$, satisfying

$$\hat{H}^\dagger \hat{\xi} = \hat{\xi} \hat{H},\quad (\text{A11})$$

where $\hat{\xi}$'s can be expressed using the spectral decomposition as

$$\hat{\xi} = \sum_n \xi_n |\xi_n\rangle \langle \xi_n| \quad (\text{A12})$$

with $\xi_n > 0$ being the eigenvalues and $|\xi_n\rangle$ the orthonormal eigenvectors. The quasi-Hermiticity Eq. (A11) implies that \hat{H} has the real spectrum, that is, it is similar to a Hermitian operator $\hat{H}_h = \hat{S}\hat{H}\hat{S}^{-1}$ that has the identical spectrum, where the similarity operator \hat{S} can be constructed as

$$\hat{S} \equiv \sum_n \sqrt{\xi_n} |\xi_n\rangle \langle \xi_n|. \quad (\text{A13})$$

The Hermiticity of \hat{H}_h can be easily proved by noting that

$$\begin{aligned}\hat{H}_h^\dagger &= \hat{S}^{-1} \hat{H}^\dagger \hat{S} = \hat{S}^{-1} (\hat{H}^\dagger \hat{\xi}) \hat{\xi}^{-1} \hat{S} = \hat{S}^{-1} (\hat{\xi} \hat{H}) \hat{S}^{-1} \\ &= \hat{S} \hat{H} \hat{S}^{-1} = \hat{H}_h,\end{aligned}\quad (\text{A14})$$

where we use the quasi-Hermiticity of \hat{H} in Eq. (A11). Thus, quasi-Hermiticity is a sufficient yet necessary condition for the reality of the spectrum.

Appendix B: The symmetries of the effective non-Hermitian Hamiltonian

In this section, we give the explicit forms of various symmetries of the effective non-Hermitian Hamiltonian \hat{H}_{NH} in the main text when $\chi_+ = \chi_- \equiv \chi$:

$$\hat{H}_{\text{NH}} \equiv \hat{\psi}^\dagger H \hat{\psi} = \sum_{k \in \text{BZ}} \hat{\psi}_k^\dagger H_k \hat{\psi}_k, \quad (\text{B1})$$

where the bases in respective real and k -spaces read

$$\hat{\psi}^\dagger \equiv (\{\hat{a}_{j\uparrow}^\dagger \hat{a}_{j\downarrow}^\dagger \hat{b}_{j\uparrow}^\dagger \hat{b}_{j\downarrow}^\dagger\}), \quad \hat{\psi} \equiv (\{\hat{a}_{j\uparrow} \hat{a}_{j\downarrow} \hat{b}_{j\uparrow} \hat{b}_{j\downarrow}\})^T, \quad (\text{B2})$$

and

$$\hat{\psi}_k^\dagger \equiv (\hat{a}_{k\uparrow}^\dagger \hat{a}_{k\downarrow}^\dagger \hat{b}_{k\uparrow}^\dagger \hat{b}_{k\downarrow}^\dagger), \quad \hat{\psi}_k \equiv (\hat{a}_{k\uparrow} \hat{a}_{k\downarrow} \hat{b}_{k\uparrow} \hat{b}_{k\downarrow})^T, \quad (\text{B3})$$

related by the discrete Fourier transform (6), and H and H_k are the corresponding coefficient matrices.

Time-reversal symmetry. Due to the reality of \hat{H}_{NH} 's parameters, the ladder respects the time-reversal symmetry:

$$\hat{T} \hat{H}_{\text{NH}} \hat{T}^{-1} = \hat{H}_{\text{NH}} \quad (\text{B4})$$

where the time-reversal operation \hat{T} acts as the complex conjugation K for numbers, preserving the operators in real space:

$$\hat{T} : \hat{a}_{j\sigma}^{(\dagger)} \rightarrow \hat{a}_{j\sigma}^{(\dagger)} K, \quad \hat{b}_{j\sigma}^{(\dagger)} \rightarrow \hat{b}_{j\sigma}^{(\dagger)} K, \quad (\text{B5})$$

and correspondingly in k -space, it reverses the sign of k accompanied by the complex conjugation:

$$\hat{T} : \hat{a}_{k\sigma}^{(\dagger)} \rightarrow \hat{a}_{-k,\sigma}^{(\dagger)} K, \quad \hat{b}_{k\sigma}^{(\dagger)} \rightarrow \hat{b}_{-k,\sigma}^{(\dagger)} K. \quad (\text{B6})$$

Thus,

$$\hat{T} \hat{\psi}_k^\dagger \hat{T}^{-1} = \hat{\psi}_k^\dagger K, \quad \hat{T} \hat{\psi}_k \hat{T}^{-1} = K \hat{\psi}_k, \quad (\text{B7})$$

and the time-reversal symmetry Eq. (B4) requires that

$$KH_kK = H_k^* = H_{-k}, \quad (\text{B8})$$

which ensures that the eigenenergies in k -space have the relation $\epsilon_{-k,m} = \epsilon_{kn}^*$, where ϵ_{kn} means the n -th eigenenergy of H_k .

Chiral symmetry. Due to the bipartition of the ladder, it has the chiral symmetry:

$$\hat{C}\hat{H}_{\text{NH}}\hat{C}^{-1} = -\hat{H}_{\text{NH}} \quad (\text{B9})$$

with the chiral operation

$$\hat{C} : \hat{a}_{j\uparrow}^{(\dagger)} \rightarrow \hat{a}_{j\uparrow}^{(\dagger)}, \hat{a}_{j\downarrow}^{(\dagger)} \rightarrow -\hat{a}_{j\downarrow}^{(\dagger)}, \hat{b}_{j\uparrow}^{(\dagger)} \rightarrow -\hat{b}_{j\uparrow}^{(\dagger)}, \hat{b}_{j\downarrow}^{(\dagger)} \rightarrow \hat{b}_{j\downarrow}^{(\dagger)} \quad (\text{B10})$$

in real space, and correspondingly

$$\hat{C} : \hat{a}_{k\uparrow}^{(\dagger)} \rightarrow \hat{a}_{k\uparrow}^{(\dagger)}, \hat{a}_{k\downarrow}^{(\dagger)} \rightarrow -\hat{a}_{k\downarrow}^{(\dagger)}, \hat{b}_{k\uparrow}^{(\dagger)} \rightarrow -\hat{b}_{k\uparrow}^{(\dagger)}, \hat{b}_{k\downarrow}^{(\dagger)} \rightarrow \hat{b}_{k\downarrow}^{(\dagger)} \quad (\text{B11})$$

in k -space. Thus,

$$\hat{C}\hat{\psi}_k^\dagger\hat{C}^{-1} = \hat{\psi}_k^\dagger C, \quad \hat{C}\hat{\psi}_k\hat{C}^{-1} = C^\dagger\hat{\psi}_k, \quad (\text{B12})$$

with

$$C = \begin{pmatrix} 1 & 0 & 0 & 0 \\ 0 & -1 & 0 & 1 \\ 0 & 0 & -1 & 0 \\ 0 & 1 & 0 & 1 \end{pmatrix} = \tau_z \otimes \sigma_z = C^\dagger = C^{-1}, \quad (\text{B13})$$

which indicates that $\hat{C}^\dagger = \hat{C}^{-1} = \hat{C}$. Hereafter, $\tau_{x,y,z}$ and $\sigma_{x,y,z}$ are both Pauli matrices acting on the sublattice (a, b) and the leg (\uparrow, \downarrow) spaces, respectively; τ_0 and σ_0 are the respective identity matrices. The chiral symmetry Eq. (B9) requires that

$$CH_kC^\dagger = -H_k, \quad (\text{B14})$$

which ensures that the eigenenergies in k -space have the relation $\epsilon_{km} = -\epsilon_{kn}$.

Pseudo-mirror symmetry. The ladder also has the pseudo-mirror symmetry:

$$\hat{M}\hat{H}_{\text{NH}}\hat{M}^{-1} = \hat{H}_{\text{NH}}^\dagger \quad (\text{B15})$$

with the mirror operation

$$\hat{M} : \hat{a}_{j\sigma}^{(\dagger)} \leftrightarrow \hat{b}_{-j,\sigma}^{(\dagger)}, \quad (\text{B16})$$

in real space, and correspondingly

$$\hat{M} : \hat{a}_{k\sigma}^{(\dagger)} \leftrightarrow \hat{b}_{-k,\sigma}^{(\dagger)}, \quad (\text{B17})$$

in k -space. Thus,

$$\hat{M}\hat{\psi}_k^\dagger\hat{M}^{-1} = \hat{\psi}_{-k}^\dagger M, \quad \hat{M}\hat{\psi}_k\hat{M}^{-1} = M\hat{\psi}_{-k}, \quad (\text{B18})$$

with

$$M = \begin{pmatrix} 0 & 0 & 1 & 0 \\ 0 & 0 & 0 & 1 \\ 1 & 0 & 0 & 0 \\ 0 & 1 & 0 & 0 \end{pmatrix} = \tau_x \otimes \sigma_0 = M^\dagger = M^{-1}, \quad (\text{B19})$$

which indicates that $\hat{M}^\dagger = \hat{M}^{-1} = \hat{M}$. The pseudo-mirror symmetry Eq. (B15) requires that

$$MH_kM = H_{-k}^\dagger, \quad (\text{B20})$$

which ensures that the eigenenergies in k -space have the relation $\epsilon_{-k,m} = \epsilon_{kn}^*$.

Inversion symmetry. The ladder also has the inversion symmetry:

$$\hat{I}\hat{H}_{\text{NH}}\hat{I}^{-1} = \hat{H}_{\text{NH}} \quad (\text{B21})$$

with the inversion operation

$$\hat{I} : \hat{a}_{j\sigma}^{(\dagger)} \rightarrow \hat{a}_{-j,\bar{\sigma}}^{(\dagger)}, \quad \hat{b}_{j\sigma}^{(\dagger)} \rightarrow \hat{b}_{-(j+1),\bar{\sigma}}^{(\dagger)}, \quad (\text{B22})$$

in real space, where $\bar{\sigma}$ means the opposite leg to leg- σ , and correspondingly

$$\hat{I} : \hat{a}_{k\sigma}^{(\dagger)} \rightarrow \hat{a}_{-k,\bar{\sigma}}^{(\dagger)}, \quad \hat{b}_{k\sigma}^\dagger \rightarrow e^{-ik}\hat{b}_{-k,\bar{\sigma}}^\dagger, \quad \hat{b}_{k\sigma} \rightarrow e^{ik}\hat{b}_{-k,\bar{\sigma}}, \quad (\text{B23})$$

in k -space. Thus,

$$\hat{I}\hat{\psi}_k^\dagger\hat{I}^{-1} = \hat{\psi}_{-k}^\dagger I_k, \quad \hat{I}\hat{\psi}_k\hat{I}^{-1} = I_k^\dagger\hat{\psi}_{-k}, \quad (\text{B24})$$

with

$$I_k = \begin{pmatrix} 0 & 1 & 0 & 0 \\ 1 & 0 & 0 & 0 \\ 0 & 0 & 0 & e^{-ik} \\ 0 & 0 & e^{-ik} & 0 \end{pmatrix} = \begin{pmatrix} 1 & 0 \\ 0 & e^{-ik} \end{pmatrix} \otimes \sigma_x, \quad (\text{B25})$$

$$I_k^\dagger = I_k^{-1} \neq I_k,$$

which indicates that $\hat{I}^\dagger = \hat{I}^{-1} = \hat{I}$. The inversion symmetry Eq. (B21) requires that

$$I_k H_k I_k^\dagger = H_{-k}, \quad (\text{B26})$$

which ensures that the eigenenergies in k -space have the relation $\epsilon_{-k,m} = \epsilon_{kn}$.

Pseudo-glide symmetry. The ladder also has the pseudo-glide symmetry:

$$\hat{G}\hat{H}_{\text{NH}}\hat{G}^{-1} = \hat{H}_{\text{NH}}^\dagger \quad (\text{B27})$$

with the pseudo-glide operation:

$$\hat{G} : \hat{a}_{j\sigma}^{(\dagger)} \rightarrow \hat{b}_{j\bar{\sigma}}^{(\dagger)}, \quad \hat{b}_{j\sigma}^{(\dagger)} \rightarrow \hat{a}_{j+1,\bar{\sigma}}^{(\dagger)}, \quad (\text{B28})$$

in real space, which also satisfies the relation $\hat{G} = \hat{M}\hat{I}$, and correspondingly

$$\hat{G} : \hat{a}_{k\sigma}^{(\dagger)} \rightarrow \hat{b}_{k\bar{\sigma}}^{(\dagger)}, \quad \hat{b}_{k\sigma}^\dagger \rightarrow e^{-ik}\hat{a}_{k\bar{\sigma}}^\dagger, \quad \hat{b}_{k\sigma} \rightarrow e^{ik}\hat{a}_{k\bar{\sigma}}, \quad (\text{B29})$$

in k -space. Thus,

$$\hat{G}\hat{\psi}_k^\dagger\hat{G}^{-1} = \hat{\psi}_k^\dagger G_k, \quad \hat{G}\hat{\psi}_k\hat{G}^{-1} = G_k^\dagger\hat{\psi}_k, \quad (\text{B30})$$

with

$$G_k = \begin{pmatrix} 0 & 0 & 0 & e^{-ik} \\ 0 & 0 & e^{-ik} & 0 \\ 0 & 1 & 0 & 0 \\ 1 & 0 & 0 & 0 \end{pmatrix} = \begin{pmatrix} 0 & e^{-ik} \\ 1 & 0 \end{pmatrix} \otimes \sigma_x = MI_k, \\ G_k^\dagger = G_k^{-1} \neq G_k, \quad G_k^2 = e^{-ik}I \quad (I : \text{identity matrix}), \quad (\text{B31})$$

which indicates that $\hat{G}^\dagger = \hat{G}^{-1} \neq \hat{G}$. The pseudo-glide symmetry Eq. (B27) requires that

$$G_k H_k G_k^\dagger = H_k^\dagger, \quad (\text{B32})$$

which ensures that the eigenenergies in k -space have the relation $\epsilon_{km} = \epsilon_{kn}^*$.

Pseudo-Hermitian symmetry. The pseudo-glide relation (B32) is close to the form of the pseudo-Hermiticity (A2), with only the violation that G_k is not Hermitian. To make up this incompleteness, we can define

$$\eta_k \equiv e^{ik/2} G_k = \begin{pmatrix} 0 & 0 & 0 & e^{-ik/2} \\ 0 & 0 & e^{-ik/2} & 0 \\ 0 & e^{ik/2} & 0 & 0 \\ e^{ik/2} & 0 & 0 & 0 \end{pmatrix} \\ = \begin{pmatrix} 0 & e^{-ik/2} \\ e^{ik/2} & 0 \end{pmatrix} \otimes \sigma_x = \eta_k^\dagger = \eta_k^{-1} \quad (\text{B33})$$

such that

$$\eta_k H_k \eta_k^{-1} = H_k^\dagger \quad (\text{B34})$$

with a Hermitian matrix η_k , that is, H_k is η_k -pseudo-Hermitian. Assuming that $\hat{\eta}$ is the pseudo-Hermitian operator, to make \hat{H}_{NH} η -pseudo-Hermitian, i.e.,

$$\hat{\eta}\hat{H}_{\text{NH}}\hat{\eta}^{-1} = \hat{H}_{\text{NH}}^\dagger, \quad (\text{B35})$$

we have

$$\hat{\eta}\hat{\psi}_k^\dagger\hat{\eta}^{-1} = \hat{\psi}_k^\dagger\eta_k, \quad \hat{\eta}\hat{\psi}_k\hat{\eta}^{-1} = \eta_k^\dagger\hat{\psi}_k, \quad (\text{B36})$$

and thus,

$$\hat{\eta} : \quad \hat{a}_{k\sigma}^\dagger \rightarrow e^{ik/2}\hat{b}_{k\bar{\sigma}}^\dagger, \quad \hat{b}_{k\sigma}^\dagger \rightarrow e^{-ik/2}\hat{a}_{k\bar{\sigma}}^\dagger, \\ \hat{a}_{k\sigma} \rightarrow e^{-ik/2}\hat{b}_{k\bar{\sigma}}, \quad \hat{b}_{k\sigma} \rightarrow e^{ik/2}\hat{a}_{k\bar{\sigma}}, \quad (\text{B37})$$

in k -space, which indicates that $\hat{\eta}^\dagger = \hat{\eta}^{-1} = \hat{\eta}$. Correspondingly, using the discrete Fourier transform (6), we obtain the operations in real space:

$$\hat{\eta} : \quad \hat{a}_{j\sigma}^\dagger \rightarrow \sum_{j'} \hat{b}_{j'\bar{\sigma}}^\dagger \eta_{j'j}, \quad \hat{b}_{j\sigma}^\dagger \rightarrow \sum_{j'} \hat{a}_{j'\bar{\sigma}}^\dagger \eta_{j'j}^*, \\ \hat{a}_{j\sigma} \rightarrow \sum_{j'} \hat{b}_{j'\bar{\sigma}} \eta_{j'j}^*, \quad \hat{b}_{j\sigma} \rightarrow \sum_{j'} \hat{a}_{j'\bar{\sigma}} \eta_{j'j}, \quad (\text{B38})$$

where

$$\eta_{j'j} = \frac{1}{L} \sum_k e^{-ik(j-j'-1/2)} \\ = \frac{2L^{-1}}{1 - \exp[-i2\pi L^{-1}(j-j'-1/2)]}. \quad (\text{B39})$$

This expression clearly demonstrates that the pseudo-Hermiticity operation is highly complex, transforming a single site of a leg to a superposition of all sites of another leg, not like the common operations such as chiral, mirror, inversion, and glide operations, which only involves single-site transformations.

When $\chi_+ \neq \chi_-$, one can follow the similar procedure to verify that the time-reversal, the chiral, and the inversion symmetries are preserved, but the pseudo-mirror, the pseudo-glide, and the η_k -pseudo-Hermitian symmetries are broken. Even in this case, the preserving symmetries are enough to ensure the D_{2h} point group of the H_k 's eigenenergies in the composite 3D space spanned by the three 2-fold rotating axes of the k -axis, the real and the imaginary axes of the complex energy plane.

Appendix C: A gauge-invariant winding number for non-Hermitian multi-band systems with chiral symmetries

Due to the chiral symmetry $\{H_k, C\} = 0$, the right/left eigenvectors of the Hamiltonian matrix H_k of dimension $2N$ appear in pairs for each k , $\{Cu_{kn}^{(r/l)}, u_{kn}^{(r/l)}\}$, with the corresponding sign-inverted eigenenergies $\{\epsilon_{kn}, -\epsilon_{kn}\}$. Thus, we can categorize these eigenvectors into two subspaces \mathbb{G}_\pm of dimension N , and define a $2N \times N$ matrix $U_-^{(r/l)} \equiv (u_{k1}^{(r/l)}, \dots, u_{kN}^{(r/l)})$ to group the eigenvectors in \mathbb{G}_- and the matrix $U_+^{(r/l)} \equiv CU_-^{(r/l)}$ in \mathbb{G}_+ , where the subscripts “ \pm ” are simply labels, as the eigenenergies are generally complex for non-Hermitian Hamiltonians. One can choose eigenvectors of the subspaces for demand, without necessarily ordering them by the real or imaginary parts of the eigenenergies. Hereafter, we assume that the defectiveness (i.e., non-diagonalization) of the non-Hermitian Hamiltonian H_k occurs only at finite discrete sets of system parameters such that the biorthogonal theory can be analytically used at the neighborhood of these points, preventing using the theory of generalized eigenvectors.

Given the biorthonormal relations between right and left eigenvectors, i.e., $U_\pm^{(l)\dagger}U_\pm^{(r)} = I_N$ and $U_\pm^{(l)\dagger}U_\mp^{(r)} = 0$, where I_N is the identity matrix of dimension N , we can define a $2N \times 2N$ matrix $U_k \equiv (U_+^{(r)}, U_-^{(r)})$ to diagonalize H_k as

$$U_k^{-1}H_kU_k = \begin{pmatrix} E_k & 0 \\ 0 & -E_k \end{pmatrix}. \quad (\text{C1})$$

where $U_k^{-1} = (U_+^{(l)}, U_-^{(l)})^\dagger$ and $E_k \equiv \text{diag}(\epsilon_{k1}, \dots, \epsilon_{kN})$. Thus, we can rewrite H_k using the eigenvectors and the

eigenenergies as

$$H_k = U_+^{(r)} E_k U_+^{(l)\dagger} - U_-^{(r)} E_k U_-^{(l)\dagger}. \quad (\text{C2})$$

Due to the chiral symmetry $\{H_k, C\} = 0$, H_k can be brought into a block off-diagonal form:

$$H_k^{(b)} \equiv U_s^{-1} H_k U_s \equiv \begin{pmatrix} 0 & h_k^{(+)} \\ h_k^{(-)} & 0 \end{pmatrix} \quad (\text{C3})$$

with two $N \times N$ matrices $h_k^{(+)}$ and $h_k^{(-)}$, under the basis represented by the unitary matrix U_s (U_s -basis) that diagonalizes C , i.e.,

$$U_s^\dagger C U_s = \begin{pmatrix} I_N & 0 \\ 0 & -I_N \end{pmatrix}. \quad (\text{C4})$$

This can be proven as follows:

$$0 = U_s^\dagger \{H_k, C\} U_s = \left\{ H_k^{(b)}, \begin{pmatrix} I_N & 0 \\ 0 & -I_N \end{pmatrix} \right\}, \quad (\text{C5})$$

which leads to

$$H_k^{(b)} = \begin{pmatrix} -I_N & 0 \\ 0 & I_N \end{pmatrix} H_k^{(b)} \begin{pmatrix} I_N & 0 \\ 0 & -I_N \end{pmatrix}. \quad (\text{C6})$$

This relation clearly shows that $H_k^{(b)}$ must be off-diagonal.

To define the topology, one can construct a Q -matrix [63] that has identical eigenvectors but with eigenvalues $\pm E_k$ of the eigenvectors in \mathbb{G}_\pm subspaces collapsed to ± 1 , respectively:

$$Q_k \equiv U_+^{(r)} U_+^{(l)\dagger} - U_-^{(r)} U_-^{(l)\dagger}. \quad (\text{C7})$$

It can be easily verified that Q_k shares the same chiral symmetry as H_k , i.e., $\{Q_k, C\} = 0$. Likewise, Q_k can also be cast in a block off-diagonal form under the same U_s -basis of $H_k^{(b)}$:

$$Q_k^{(b)} \equiv U_s^\dagger Q_k U_s \equiv \begin{pmatrix} 0 & q_k \\ q_k^{-1} & 0 \end{pmatrix} \quad (\text{C8})$$

where q_k is an $N \times N$ invertible matrix (i.e., $\det q_k \neq 0$). That the two block matrices are invertible to each other is derived from $[Q_k^{(b)}]^2 = Q_k^2 = I_{2N}$. Then, we can define the winding number:

$$w \equiv \frac{1}{2\pi i} \int_{k \in \text{BZ}} \text{tr} q_k^{-1} dq_k = \frac{1}{2\pi i} \int_{k \in \text{BZ}} d \ln \det q_k. \quad (\text{C9})$$

Here, the second identity can be obtained using the following relation:

$$\begin{aligned} \text{tr} q_k^{-1} dq_k &= \text{tr} U \Lambda^{-1} U^{-1} d U \Lambda U^{-1} = \text{tr} \Lambda^{-1} d \Lambda \\ &= d \text{tr} \ln \Lambda = d \ln \det \Lambda = d \ln \det U \Lambda U^{-1} \\ &= d \ln \det q_k, \end{aligned} \quad (\text{C10})$$

where we use the eigenvalue decomposition $U^{-1} q_k U = \Lambda \equiv \text{diag}(\{\lambda_s\})$ with λ_s ($s = 1, \dots, N$) being the eigenvalues, and $\ln \Lambda \equiv \text{diag}(\{\ln \lambda_s\})$. This winding number w defines a map from $k \in S^1$ onto an $N \times N$ invertible matrix $q_k \in GL(N, \mathbb{C})$ to reflect the topology of the bipartition of the Hilbert space into two subspaces \mathbb{G}_\pm in BZ. This map is a fundamental homotopy group $\pi_1(GL(N, \mathbb{C})) \in \mathbb{Z}$. Specifically, when H_k and thus Q_k and $Q_k^{(b)}$ are Hermitian, the invertible matrix q_k becomes unitary (i.e., $q_k^\dagger = q_k^{-1}$), reducing the fundamental homotopy group from $\pi_1(GL(N, \mathbb{C}))$ to $\pi_1(U(N)) \in \mathbb{Z}$.

It is important to note that given the U_s -basis, which changes q_k but preserves w due to the independence of U_s on k , the block matrix q_k and thus the winding number w are invariant with respect to any local (i.e., k -dependent) invertible linear transformation R_k of the eigenvectors in each subspace, i.e., $\tilde{U}_\pm^{(r)} = U_\pm^{(r)} R_k$ and $\tilde{U}_\pm^{(l)\dagger} = R_k^{-1} U_\pm^{(l)\dagger}$. This gauge invariance reflects the robustness of the winding number w , provided that the two sets of bands do not touch for any k in BZ. Apparently, this gauge invariance does not hold for $h_k^{(+)}$ or $h_k^{(-)}$, and thus, the winding number cannot be properly defined using them.

To explicitly express q_k , we rewrite the eigenvectors under the U_s -basis as $U_s^\dagger U_{\pm}^{(r/l)} \equiv (U_1^{(r/l)}; U_2^{(r/l)})$, where the two $N \times N$ matrices $U_{1,2}^{(r/l)}$ are arranged in a vertical order, denoted by “;” in the parentheses. According to the biorthonormal and completeness relations:

$$\begin{aligned} I_N &= [U_-^{(l)\dagger} U_s][U_s^\dagger U_-^{(r)}] = U_1^{(l)\dagger} U_1^{(r)} + U_2^{(l)\dagger} U_2^{(r)} \\ 0 &= [U_+^{(l)\dagger} U_s][U_s^\dagger U_-^{(r)}] = U_1^{(l)\dagger} U_1^{(r)} - U_2^{(l)\dagger} U_2^{(r)} \\ I_{2N} &= U_s^\dagger [U_+^{(r)} U_+^{(l)\dagger} + U_-^{(r)} U_-^{(l)\dagger}] U_s \\ &= \begin{pmatrix} 2U_1^{(r)} U_1^{(l)\dagger} & 0 \\ 0 & 2U_2^{(r)} U_2^{(l)\dagger} \end{pmatrix}, \end{aligned} \quad (\text{C11})$$

one can immediately obtain

$$U_{1,2}^{(l)\dagger} U_{1,2}^{(r)} = U_{1,2}^{(r)} U_{1,2}^{(l)\dagger} = \frac{I_N}{2}. \quad (\text{C12})$$

From Eqs. (C7) and (C8), one has

$$\begin{aligned} Q_k^{(b)} &= U_s^\dagger [C U_-^{(r)} U_-^{(l)\dagger} C - U_-^{(r)} U_-^{(l)\dagger}] U_s \\ &= \begin{pmatrix} I_N & 0 \\ 0 & -I_N \end{pmatrix} U_s^\dagger U_-^{(r)} U_-^{(l)\dagger} U_s \begin{pmatrix} I_N & 0 \\ 0 & -I_N \end{pmatrix} \\ &\quad - U_s^\dagger U_-^{(r)} U_-^{(l)\dagger} U_s \\ &= \begin{pmatrix} 0 & -2U_1^{(r)} U_2^{(l)\dagger} \\ -2U_2^{(r)} U_1^{(l)\dagger} & 0 \end{pmatrix}. \end{aligned} \quad (\text{C13})$$

Thus,

$$q_k = -2U_1^{(r)} U_2^{(l)\dagger}, \quad q_k^{-1} = -2U_2^{(r)} U_1^{(l)\dagger}, \quad (\text{C14})$$

which are apparently gauge invariant. These expressions offer a way of numerically calculating the winding number (C9) with eigenvectors.

Using these expressions of q_k and q_k^{-1} as well as the above relations, the winding number can be further calculated as

$$\begin{aligned}
w &= \frac{1}{2\pi i} \int_{k \in \text{BZ}} \text{tr} q_k^{-1} dq_k \\
&= \frac{1}{\pi i} \int_{k \in \text{BZ}} \text{tr} [U_1^{(l)\dagger} dU_1^{(r)} - U_2^{(l)\dagger} dU_2^{(r)}] \\
&= \frac{1}{\pi i} \int_{k \in \text{BZ}} \text{tr} U_+^{(l)\dagger} dU_-^{(r)} \\
&= \frac{1}{\pi i} \int_{k \in \text{BZ}} \text{tr} U_-^{(l)\dagger} C dU_-^{(r)}, \tag{C15}
\end{aligned}$$

which can be regarded as an alternative definition of the gauge-independent winding number using eigenvectors in two subspaces. The C matrix is the key to immune to the gauge change, which leads to the essential difference to the winding number defined using eigenvectors in only one subspace, say

$$\begin{aligned}
w_- &\equiv \frac{1}{\pi i} \int_{k \in \text{BZ}} \text{tr} U_-^{(l)\dagger} dU_-^{(r)} \\
&= \frac{1}{\pi} \int_{k \in \text{BZ}} \text{tr} A_k^{(-)} = \frac{\varphi_{\text{Zak}}}{\pi}. \tag{C16}
\end{aligned}$$

Here, $\varphi_{\text{Zak}} \equiv \int_{k \in \text{BZ}} \text{tr} A_k^{(-)}$ is the Zak phase defined in BZ for the subspace \mathbb{G}_- using the non-Abelian Berry connection $A_k^{(-)} \equiv -iU_-^{(l)\dagger} dU_-^{(r)}$. This definition is not gauge invariant, since

$$\begin{aligned}
\tilde{w}_- &= \frac{1}{\pi i} \int_{k \in \text{BZ}} \text{tr} \tilde{U}_-^{(l)\dagger} d\tilde{U}_-^{(r)} \\
&= w_- + \frac{1}{\pi i} \int_{k \in \text{BZ}} \text{tr} R_k^{-1} dR_k \\
&= w_- + \frac{1}{\pi i} \int_{k \in \text{BZ}} \text{tr} d \ln \Lambda \\
&= w_- + \frac{1}{\pi i} \sum_{n=1}^N \int_{k \in \text{BZ}} (d \ln r_n + id\varphi_n) \\
&= w_- + \frac{1}{\pi} \sum_{n=1}^N \int_{k \in \text{BZ}} d\varphi_n \\
&= w_- + 2 \times \text{Integer}, \tag{C17}
\end{aligned}$$

where we use the same trick as in Eq. (C10), $U^{-1}R_kU = \Lambda \equiv \text{diag}\{r_n e^{i\varphi_n}\}$ ($n = 1, \dots, N$) with $r_n \geq 0$ and $\varphi_n \in \mathbb{R}$, and notice that r_n is periodic in k but φ_n is periodic modulo 2π , since R_k is a periodic function of k . Eq. (C17) demonstrates that this definition of winding number is only valid modulo 2, i.e., $w_- \in \mathbb{Z}_2$, much coarser than $w \in \mathbb{Z}$. It is interesting to note that the two kinds of winding numbers come from different parts of the matrix of the non-Hermitian non-Abelian Berry connection for the whole bands:

$$A_k \equiv -iU_k^{-1} dU_k = \begin{pmatrix} -iU_+^{(l)\dagger} dU_+^{(r)} & -iU_+^{(l)\dagger} dU_-^{(r)} \\ -iU_-^{(l)\dagger} dU_+^{(r)} & -iU_-^{(l)\dagger} dU_-^{(r)} \end{pmatrix}. \tag{C18}$$

From the point of view of H_k , one can also construct $H_k^{(b)}$ as in Eq. (C13):

$$\begin{aligned}
H_k^{(b)} &= U_s^\dagger [CU_-^{(r)} E_k U_-^{(l)\dagger} C - U_-^{(r)} E_k U_-^{(l)\dagger}] U_s \\
&= \begin{pmatrix} 0 & -2U_1^{(r)} E_k U_2^{(l)\dagger} \\ -2U_2^{(r)} E_k U_1^{(l)\dagger} & 0 \end{pmatrix} \tag{C19}
\end{aligned}$$

Thus,

$$h_k^{(+)} = -2U_1^{(r)} E_k U_2^{(l)\dagger}, \quad h_k^{(-)} = -2U_2^{(r)} E_k U_1^{(l)\dagger}, \tag{C20}$$

which apparently are both gauge dependent. Combined with Eq. (C14), we have the relations between q_k and $h_k^{(\pm)}$:

$$q_k = h_k^{(+)} [U_2^{(l)\dagger}]^{-1} E_k^{-1} U_2^{(l)\dagger} = [U_1^{(l)\dagger}]^{-1} E_k U_1^{(l)\dagger} h_k'^{-1}, \tag{C21}$$

and thus, the winding number (C9) can be reexpressed as

$$\begin{aligned}
w &= \frac{1}{2\pi i} \int_{k \in \text{BZ}} d \ln \det q_k \\
&= \frac{1}{2\pi i} \int_{k \in \text{BZ}} d \ln \det h_k^{(+)} - \frac{1}{2\pi i} \int_{k \in \text{BZ}} d \ln \det E_k \\
&= -\frac{1}{2\pi i} \int_{k \in \text{BZ}} d \ln \det h_k^{(-)} + \frac{1}{2\pi i} \int_{k \in \text{BZ}} d \ln \det E_k. \tag{C22}
\end{aligned}$$

These expressions demonstrate that if one tries to calculate the gauge-invariant winding number using either $h_k^{(+)}$ or $h_k^{(-)}$, the complex eigenenergies E_k of the non-Hermitian systems must be involved simultaneously, which in Hermitian systems does not contribute due to the reality of energies and reduces to the traditional expression. For the energy spectrum that respects the mirror symmetry for each k , there always exist counter-rotating traces of eigenenergies along with k , and thus the energy term in Eq. (C22) must vanish; for the energy spectrum separated by a line gap, the energy term also vanishes because the origin of the complex energy plane is not enclosed; for the energy spectrum separated by a point gap enclosing the origin but not respecting the mirror symmetry, the energy term must be carefully considered. Note that although $h_k^{(\pm)}$ is gauge dependent, $\det h_k^{(\pm)}$ is not and thus, the $h_k^{(\pm)}$ part in Eq. (C22) is still gauge invariant, which can be used as another definition of gauge-invariant winding numbers:

$$\begin{aligned}
w_h^{(\pm)} &\equiv \frac{1}{2\pi i} \int_{k \in \text{BZ}} \text{tr} [h_k^{(\pm)}]^{-1} dh_k^{(\pm)} \\
&= \frac{1}{2\pi i} \int_{k \in \text{BZ}} d \ln \det h_k^{(\pm)}. \tag{C23}
\end{aligned}$$

The winding number $w_h^{(\pm)}$ also defines a map from $k \in S^1$ onto an $N \times N$ invertible matrix $h_k^{(\pm)} \in GL(N, \mathbb{C})$, also corresponding to a fundamental homotopy group

$\pi_1(GL(N, \mathbb{C})) \in \mathbb{Z}$. The difference between w and $w_h^{(\pm)}$ is whether considering the contribution from the winding of the complex eigenenergies.

To easily calculate w with only the system parameters $h_k^{(\pm)}$, the winding number can be rewritten in a more delicate way by adding the last two lines of Eq. (C22), yielding

$$\begin{aligned} w &= \frac{1}{4\pi i} \int_{k \in \text{BZ}} \left[d \ln \det h_k^{(+)} - d \ln \det h_k^{(-)} \right] \\ &= \frac{1}{2} [w_h^{(+)} - w_h^{(-)}]. \end{aligned} \quad (\text{C24})$$

The following lists more possibly useful relations for understanding the properties of this winding number:

$$\frac{\det h_k^{(+)}}{\det h_k^{(-)}} = (\det q_k)^2, \quad \det h_k^{(+)} \det h_k^{(-)} = (\det E_k)^2. \quad (\text{C25})$$

Appendix D: The relation between the dynamics and the Wilson line for non-Hermitian systems

When we add an external constant force F along, say, the right direction of the ladder, the time-dependent Schrödinger equation becomes ($\hbar = 1$) [7]

$$i\partial_t |\psi(t)\rangle = (\hat{H}_{\text{HN}} - F\hat{X}) |\psi(t)\rangle, \quad (\text{D1})$$

where $\partial_t \equiv \partial/\partial t$ and for simplicity the position operator \hat{X} is defined with respect to the positions of unit cells:

$$\hat{X} : \hat{a}_{j\sigma}^{(\dagger)} \rightarrow j\hat{a}_{j\sigma}^{(\dagger)}, \quad \hat{b}_{j\sigma}^{(\dagger)} \rightarrow j\hat{b}_{j\sigma}^{(\dagger)} \quad (\text{D2})$$

in real space, and correspondingly

$$\hat{X} : \hat{\psi}_k^\dagger \rightarrow -i\partial_k \hat{\psi}_k^\dagger, \quad \hat{\psi}_k \rightarrow i\partial_k \hat{\psi}_k, \quad (\text{D3})$$

in k -space with $\partial_k \equiv \partial/\partial k$. We rewrite the Hamiltonian (B1) in the diagonal form as

$$\hat{H}_{\text{HN}} = \sum_{k \in \text{BZ}} \hat{u}_k^{(r)\dagger} \Lambda_k \hat{u}_k^{(l)} = \sum_{k \in \text{BZ}} \sum_{n=1}^4 \epsilon_{kn} \hat{u}_{kn}^{(r)\dagger} \hat{u}_{kn}^{(l)}, \quad (\text{D4})$$

where $\hat{u}_k^{(r)\dagger} \equiv (\hat{u}_{k1}^{(r)\dagger}, \hat{u}_{k2}^{(r)\dagger}, \hat{u}_{k3}^{(r)\dagger}, \hat{u}_{k4}^{(r)\dagger}) = \hat{\psi}_k^\dagger U_k$, $\hat{u}_k^{(l)} \equiv (\hat{u}_{k1}^{(l)}, \hat{u}_{k2}^{(l)}, \hat{u}_{k3}^{(l)}, \hat{u}_{k4}^{(l)})^T = U_k^{-1} \hat{\psi}_k$, and $\Lambda_k = \text{diag}(\epsilon_{k1}, \epsilon_{k2}, \epsilon_{k3}, \epsilon_{k4})$. We set the initial state as a superposition of the Bloch states at k_0 , i.e., $|\psi(0)\rangle = \hat{u}_{k_0}^{(r)\dagger} \alpha(0) |0\rangle$, where the coefficient vector $\alpha(t) = (\alpha_1(t), \alpha_2(t), \alpha_3(t), \alpha_4(t))^T$ with $\alpha_n(t)$ being the amplitude of the Bloch state in the n th band at time t , and we normalize the coefficients at $t = 0$ by $\sum_n |\alpha_n(0)|^2 = 1$. With the ansatz that the initial state uniformly evolves to another superposition state $|\psi(t)\rangle = \hat{u}_{k(t)}^\dagger \alpha(t) |0\rangle$ at $k(t) = k_0 + Ft$, using Eq. (D1) we have the following equations of motion:

$$i\partial_t \alpha(t) = [\Lambda_{k(t)} + FA_{k(t)}] \alpha(t), \quad (\text{D5})$$

where

$$A_{k(t)} = -iU_k^{-1} \partial_k U_k \Big|_{k=k(t)} \quad (\text{D6})$$

is just the non-Hermitian non-Abelian Berry connection Eq. (C18) for the whole bands. The solution to Eq. (D5) is

$$\begin{aligned} \alpha(t) &= \mathcal{T} \exp \left\{ -i \int_0^t dt [\Lambda_{k(t)} + FA_{k(t)}] \right\} \alpha(0) \\ &= \mathcal{P} \exp \left\{ -i \int_{k_0}^{k_f} dk (\Lambda_k/F + A_k) \right\} \alpha(0) \\ &\equiv V_{k_0 \rightarrow k_f} \alpha(0), \end{aligned} \quad (\text{D7})$$

where \mathcal{T} and \mathcal{P} are the time-ordered and the path-ordered operators, respectively.

To numerically solve this equation, we divide the path $k_0 \rightarrow k_f$ into l pieces of equal intervals of length $dk = (k_f - k_0)/l$. When $l \rightarrow \infty$ (i.e., $dk \rightarrow 0$), using the relation

$$\begin{aligned} e^{-i(\Lambda_k/F + A_k)dk} &\approx e^{-i\Lambda_k dk/F} e^{-iA_k dk} \\ &\approx e^{-i\Lambda_k dk/F} (I - iA_k dk) \\ &= e^{-i\Lambda_k dk/F} (I - U_k^{-1} dU_k) \\ &= e^{-i\Lambda_k dk/F} (I + dU_k^{-1} U_k) \\ &\approx e^{-i\Lambda_k dk/F} [I + (U_{k+dk}^{-1} - U_k^{-1}) U_k] \\ &= e^{-i\Lambda_k dk/F} U_{k+dk}^{-1} U_k, \end{aligned} \quad (\text{D8})$$

we have

$$\begin{aligned} V_{k_0 \rightarrow k_f} &= e^{-i\Lambda_{k_f} dk/F} U_{k_f}^{-1} U_{k_{l-1}} \cdots e^{-i\Lambda_{k_i} dk/F} U_{k_i}^{-1} U_{k_{i-1}} \\ &\quad \cdots e^{-i\Lambda_{k_1} dk/F} U_{k_1}^{-1} U_{k_0}. \end{aligned} \quad (\text{D9})$$

where (k_1, \dots, k_{l-1}) are the $l-1$ joint points of the l pieces of equal intervals along the path.

When F is much larger than the total band width w_4 , the non-Hermitian non-Abelian Berry connection A_k dominates the evolution (i.e., $\Lambda_k/F \rightarrow 0$), yielding

$$\alpha(t) \approx \mathcal{P} \exp \left[-i \int_{k_0}^{k_f} dk A_k \right] \alpha(0) \equiv W_{k_0 \rightarrow k_f} \alpha(0), \quad (\text{D10})$$

where

$$W_{k_0 \rightarrow k_f} = U_{k_f}^{-1} U_{k_{l-1}} \cdots U_{k_i}^{-1} U_{k_{i-1}} \cdots U_{k_1}^{-1} U_{k_0} = U_k^{-1} U_{k_0}. \quad (\text{D11})$$

is a four-band Wilson line for non-Hermitian systems along the path from k_0 to k_f in k -space [50], reduced from $V_{k_0 \rightarrow k_f}$ in Eq. (D9). This Wilson line defined using the biorthonormal basis is a non-Hermitian generalization of the Wilson line in Hermitian systems [7, 9]. Apparently, $W_{k_f \rightarrow k_0} = W_{k_0 \rightarrow k_f}^{-1}$. If $k_f = k_0 + 2\pi n$ ($n \in \text{Integer}$), the Wilson line becomes a Wilson loop due to the periodicity of the BZ, and thus, $W_{k_0 \rightarrow k_0 + 2\pi n} = I$, indicating the state returns to the initial state, i.e., $|\psi(t)\rangle = |\psi(0)\rangle$.

When the force F is much larger than the maximum energy difference w_2 of the lowest two bands and smaller than the gap Δ to the other two bands, Eq. (D7) can be approximately decoupled into two independent evolutions in each subspace:

$$\begin{aligned}\alpha^{(\pm)}(t) &\approx \mathcal{P} \exp \left[-i \int_{k_0}^{k_f} dk A_k^{(\pm)} \right] \alpha^{(\pm)}(0) \\ &\equiv W_{k_0 \rightarrow k_f}^{(\pm)} \alpha^{(\pm)}(0),\end{aligned}\quad (\text{D12})$$

where (\pm) means the upper/lower 2×2 diagonal blocks in the labeled matrices and 2×1 blocks in labeled column vectors, and $W_{k_0 \rightarrow k_f}^{(\pm)}$ are the two-band Wilson lines for non-Hermitian systems in corresponding subspaces.

Likewise, $W_{k_0 \rightarrow k_f}^{(\pm)}$ can also be numerically calculated as follows:

$$\begin{aligned}W_{k_0 \rightarrow k}^{(\pm)} &= U_{\pm, k}^{(l)\dagger} U_{\pm, k_{l-1}}^{(r)} \cdots U_{\pm, k_i}^{(l)\dagger} U_{\pm, k_{i-1}}^{(r)} \cdots U_{\pm, k_1}^{(l)\dagger} U_{\pm, k_0}^{(r)} \\ &= U_{\pm, k}^{(l)\dagger} P_{\pm, k_{l-1}} \cdots P_{\pm, k_i} \cdots P_{\pm, k_1} U_{\pm, k_0}^{(r)},\end{aligned}\quad (\text{D13})$$

where $P_{\pm, k_i} \equiv U_{\pm, k_i}^{(r)} U_{\pm, k_i}^{(l)\dagger}$ is the projection matrix to the lowest/highest two bands at k_i . Apparently, the Wilson loop (i.e., $k = k_0$) is immune to the local similarity transformations in the subspace due to the invariance of the projection matrices to the transformations [50]. Note that the phase accumulation of the Wilson loop $W_{k_0 \rightarrow k_0 + 2\pi}^{(-)}$ is just the Zak phase defined in Eq. (C16), i.e., $\varphi_{\text{Zak}} = i \ln \det W_{k_0 \rightarrow k_0 + 2\pi}^{(-)}$.